



Available online at www.sciencedirect.com

ScienceDirect

Geochimica et Cosmochimica Acta 316 (2022) 363-383

Geochimica et Cosmochimica Acta

www.elsevier.com/locate/gca

Hydrological and thermodynamic controls on late Holocene gypsum formation by mixing saline groundwater and Dead Sea brine

Nurit Weber ^{a,b,*}, Gilad Antler ^{c,d}, Boaz Lazar ^a, Mordechai Stein ^{a,b}, Yoseph Yechieli ^b, Ittai Gavrieli ^b

^a The Fredy and Nadine Herrmann Institute of Earth Sciences, The Hebrew University of Jerusalem, The Edmund Safra Campus, Givat-Ram, Jerusalem 9190401, Israel

^b Geological Survey of Israel, 32 Yesha'ayahu Leibowitz St., Jerusalem 9692100, Israel ^c Department of Earth and Environmental Sciences, Ben-Gurion University of the Negev, Beersheba 8410501, Israel ^d The Interuniversity Institute for Marine Sciences, Eilat 8810302, Israel

Received 30 January 2021; accepted in revised form 1 October 2021; Available online 12 October 2021

Abstract

The rapid retreat of the Dead Sea during the past four decades led to the exposure of unique structures of massive gypsum along the shores. Many of these structures (having the shape of mounds) are associated with the activity of Ein Qedem-type saline springs that currently discharge Ca-chloride brine to the lake. Field observations, radiocarbon dating of aragonite (within the gypsum mounds) that yield ancient ages, and the narrow range of δ^{34} S and δ^{18} O values (δ^{34} S_{gyp}: 14.1–16.9‰; δ^{18} O_{gyp}: 14.4–16.5‰) indicates that the formation of the gypsum structures is related to the mixing of brines: the Dead Sea brine and ancient (last glacial) Ein Qedem type brine. These are Ca-chloride brines having different salinities and sulfur concentrations that satisfy conditions of an outsalting process whereby supersaturation of gypsum is attained by the mixing of these two brines in the offshore shallow water environment.

Thermodynamic calculations (using the PHREEQC software) show that gypsum outsalting occurred when both brines were enriched with sulfate as compared to the present. The Ein-Qedem brine had higher sulfate when subjected to less intensive bacterial sulfate reduction. The Dead Sea was characterized by higher sulfate concentrations during intervals of low lake stands. The conditions of higher sulfate concentrations and enhanced discharge of the saline springs occurred repeatedly in the Dead Sea between ~6.6 to 0.6 ka and were intermittent with periods of enhanced supply of sulfate to the lake by freshwaters. © 2021 Elsevier Ltd. All rights reserved.

Keywords: Lacustrine Gypsum; Brines; Saline springs; Dead Sea; Outsalting; Hydroclimate; Thermodynamic modeling

E-mail address: nurit.weber@mail.huji.ac.il (N. Weber).

1. INTRODUCTION

Massive gypsum deposits are found in marine or terrestrial (lacustrine) environments worldwide (e.g., Warren, 2016 and references therein). Excess evaporation in marine lagoonal-type basins (e.g., Warren, 1982; Babel, 2007) and in saline lakes (e.g., Smoot and Lowenstein, 1991) is the mechanism attributed to the formation of the gypsum

^{*} Corresponding author at: The Fredy and Nadine Herrmann Institute of Earth Sciences, The Hebrew University of Jerusalem, The Edmund Safra Campus, Givat-Ram, Jerusalem 9190401, Israel.

deposits. In lacustrine environments gypsum formation has been related to the hydrologic and limnological regime, e.g., rate of evaporation and meteoric water supply, the limnological configuration (e.g., stratified or overturned lake), and bacterial activity (e.g., bacterial sulfate reduction has been suggested to control gypsum formation in the hypersaline Lake Lisan, see Torfstein et al., 2005; Torfstein et al., 2008).

In this study, we describe a unique and, so far, an undescribed additional mechanism of gypsum formation in the lacustrine environment of the late Holocene hypersaline Dead Sea. This mechanism involves the mixing of sulfatebearing brines with variable salinities. The mixing of the two brines results in a high degree of supersaturation and massive crystallization termed outsalting. This "outsalting" process has been described for the formation of halite in the Dead Sea, where the residual brine that returns from the industrial evaporation ponds mixes with the modern Dead Sea brine (Beyth et al. 1997). Outsalting is also the proposed mechanism that controls gypsum precipitation in the Dead Sea if its brines would mix with Red Sea water (e.g., the proposed Red Sea-Dead Sea Conduit (Katz et al., 1981; Reznik et al., 2009a). However, outsalting has not been described in the past as a potential mechanism for natural massive gypsum precipitation.

The gypsum structures described and discussed in this work are located very close to hot saline springs, which currently discharge Ca-chloride brine to the Dead Sea, e.g., the Ein Qedem springs system (Fig. 1), calling for a potential role of the springs in the formation of the gypsum (Weber et al., 2021). Two gypsum facies appear at the Ein Oedem shore: 1. Stratigraphic (concordant) massive gypsum deposited on an erosional unconformity in the last glacial Lisan Formation (e.g., termed "Cape Qedem", Fig. 2A); 2. Discordant gypsum "mounds" that are pitted along the shores and appear also on the stratigraphic gypsum (Fig. 2B, Weber et al., 2021). Both facies represent a unique sedimentological setting where the Ein Qedem and the Dead Sea brines mix underwater (see Weber et al., 2021). Here, we describe the sulfur and oxygen isotope compositions of the gypsum deposits and develop a thermodynamic model to describe the outsalting process that controls their deposition. This model and the reconstruction of the environment of deposition provide new insights into the Holocene activity of the saline springs and their relation to the regional hydrology.

2. GEOLOGICAL AND GEOCHEMICAL SETTING

The modern Dead Sea is a terminal hypersaline water-body (current salinity of $\sim 350~\rm g\cdot L^{-1}$) having a unique Ca-chloride brine composition. Ca-chloride brine (as defined by Starinsky, 1974 and see also Katz and Starinsky, 2009) contains equivalent (ionic charge concentrations) ratios of Na⁺/Cl⁻<1 and Ca²⁺/(SO₄²⁻+HCO₃⁻) > 1, meaning that chloride is in excess over sodium (representing dissolved halite) and calcium is in excess over SO_4^{2-} +HCO₃⁻ (representing dissolved gypsum and CaCO₃). This brine evolved from evaporated seawater that filled the late Neogene Sedom Lagoon, which channeled Mediter-

ranean Sea waters to the Dead Sea Basin. The evaporated seawater percolated into the Judea Group aquifer, modified to Ca-chloride brines by water-rock interaction processes such as dolomitization, and returned to the lagoon (Zak, 1967; Starinsky, 1974; Stein et al., 2000, 2002). After the disconnection of the lagoon from the open sea (~3 Ma, Torfstein et al., 2009), the vast hypersaline groundwater reservoir fed a series of hypersaline terminal lakes (Katz and Starinsky, 2009). These lakes had highly variable chemical compositions and fluctuating water levels, reflecting the mixing between the Ca-chloride brines and freshwaters (Stein, 2001). The latest (Holocene) expression of these Ca-chloride brines is the modern Dead Sea and the Ein Qedem hot saline springs discharging along the central part of its western shores (Mazor and Mero, 1969; Gavrieli et al., 2001; Gavrieli and Stein, 2006; Torfstein et al., 2008, Weber et al., 2018).

The sediments deposited in the Holocene Dead Sea (past 11 kyr) comprise the Ze'elim Formation (Yechieli et al., 1993; Bookman et al., 2004). The Ze'elim Formation consists mostly of sequences of silty detritus material, mainly made up of quartz and calcite (Haliva-Cohen et al., 2012), termed here "muds": sequences of couplets of silty detritus and primary aragonite and triplets of detritus, aragonite and gypsum (the *aad facies* described by Machlus et al., 2000 and the *MAG facies* described by Migowski et al., 2006).

Ca-chloride brines similar in composition to the Dead Sea and with variable salinities are discharged along the western shores of the lake (e.g., Ein Qedem, Ein Shalem -Mineral Spa, Ein Gedi Spa, Fig. 1B). The Ein Oedem springs system currently discharging from the alluvial aquifer at the western shore of the Dead Sea is the subaerial expression of a large saline groundwater body of Ca-chloride brine (termed Qedem-Shalem brine in Gavrieli et al., 2001; Weber et al., 2018, 2021). A previous survey along the shore traced the Ein Qedem type brine to Einot Zugim in the northern part of the Dead Sea (Gavrieli et al., 2001). Weber et al. (2018) proposed that the saline groundwater that is currently discharged at Ein Qedem represent the epilimnetic (upper) brine layer of the last glacial Lake Lisan. The epilimnetic brine intruded the adjacent aquifers during the high stand period of the lake (\sim 200 \pm 30 m bmsl (below mean sea level)), between \sim 30 and 17.4 ka. After the retreat of Lake Lisan from its high stand, this brine was recycled back to the lake via the Ein Qedem saline springs (Weber et al., 2021). The recycling of the Ca-chloride brine is controlled by the hydrological regime in the Dead Sea watershed that impacted the hydrological head (affecting the flow in the Mountain aquifer) and the lake's level. The saline groundwater could discharge back to the lake by lowering the hydrological head (Shalev and Yechieli, 2007; Weber et al., 2018).

The Dead Sea Ca-chloride brine is sulfate depleted (i.e., very low SO_4^{2-}/Ca^{2+} molar ratio of ~ 0.009). This depletion possibly relates to massive deposition of gypsum in the Jordan Valley at the late Miocene (when Lake Bira filled the northern valleys of Israel, Rozenbaum et al., 2019). Dolomitization of the Mesozoic marine limestones replenished the brine with Ca^{2+} and enabled gypsum to

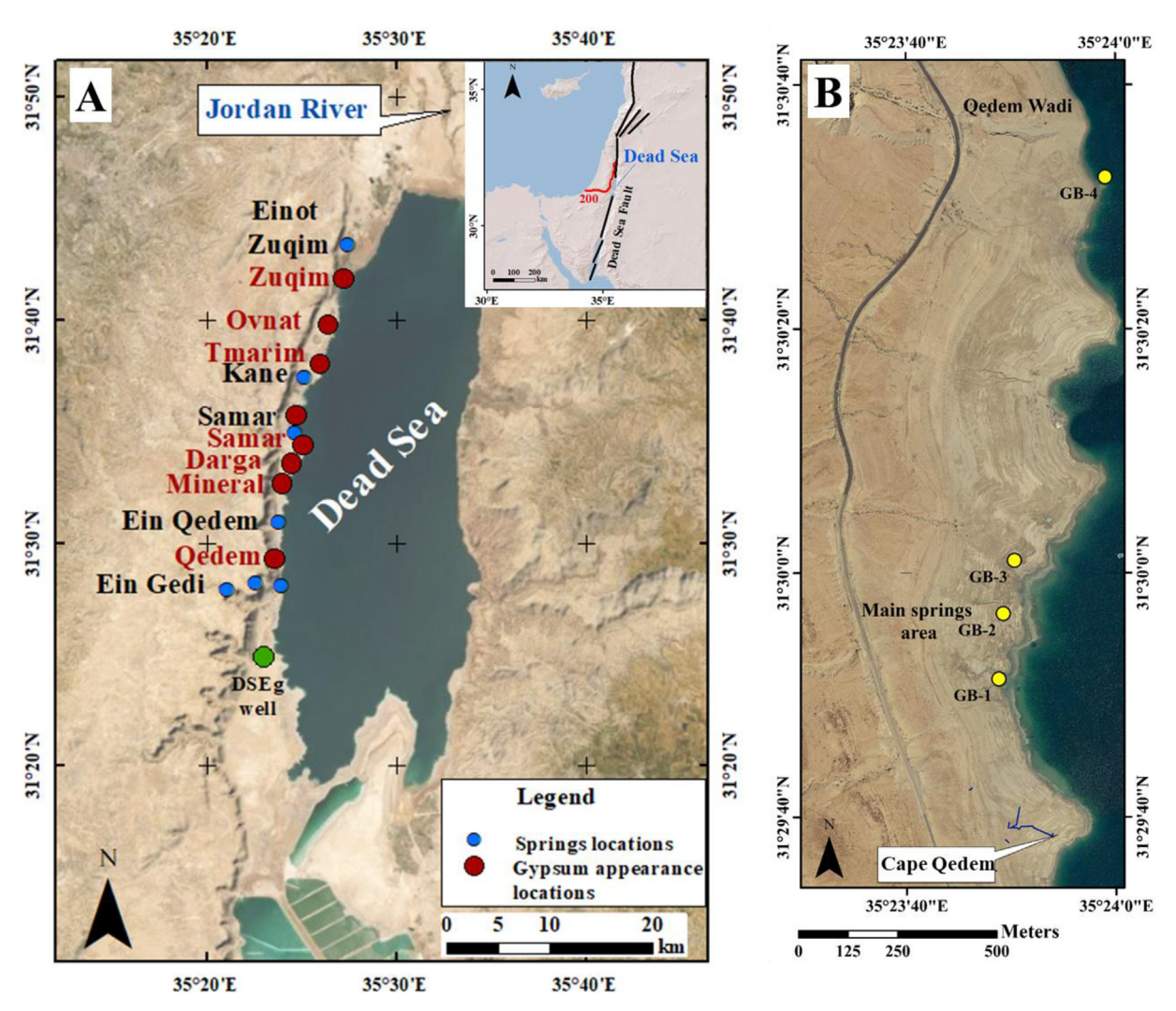


Fig. 1. Satellite pictures showing the locations of the study sites: (A) Springs (blue dots) and gypsum structures (red dots) along the western shore of the Dead Sea and the Ein Gedi (DSEg) drilling site (green). Inset: The Dead Sea Basin located along the Dead Sea Transform Fault (black line), showing the transition between the Mediterranean and the desert climate zones along the annual 200 mm isopleth (red line). (B) Ein Qedem shore showing Cape Qedem and the nearby sampled gypsum structures (yellow dots).

precipitate from the otherwise low-Ca²⁺ marine-derived brine (Gavrieli and Stein, 2006). Later, gypsum was mainly precipitated from the Quaternary lakes: Amora and Lisan, during relatively arid periods due to focusing of the sulfate and lake level retreat and overturn (Stein et al., 1997). Gypsum comprises an essential constituent of the Dead Sea lacustrine formations. The low concentration of sulfate in the Ca-chloride brine requires the addition of sulfate by freshwater to maintain gypsum deposition (Torfstein et al., 2005, 2008). The appearance of the detritusaragonite-gypsum triplets in the late Holocene (past 3000 yr) interval of the Ze'elim Formation (Migowski et al., 2006) attest to a constant supply of bicarbonate and sulfate with the freshwater inflow to the lake (Belmaker et al., 2019).

Before the last Dead Sea overturn of 1979 (Steinhorn et al., 1979), the isotopic composition of sulfate of its hypolimnion was ca. 14.5‰, about 2‰ higher than its

epilimnion (Nissenbaum and Kaplan, 1976). This was the result of bacterial sulfate reduction (BSR) in the hypolimnion and sedimentary porewater (Lerman, 1967; Nissenbaum and Kaplan, 1976). By the end of the 1950s and in the early 1960s (before the lake overturn), when the Dead Sea was stratified and already experienced negative water balance, gypsum was precipitating in the epilimnion and was accumulating above the shallow parts of the lakes (Neev and Emery, 1967). The $\delta^{34}S_{gyp}$ ($\delta^{34}S$ of that gypsum) was higher than that of the Dead Sea brine by ~2.5% (Nissenbaum and Kaplan, 1976). BSR also occurs within the coastal aquifer, as has been suggested from the high sulfide concentrations and high $\delta^{18}O_{SO4}$ and $\delta^{34}S_{SO4}$ (isotopic composition of oxygen and sulfur, respectively, in the dissolved sulfate; Gavrieli et al., 2001; Avrahamov et al., 2014). The groundwater's degree of saturation with respect to gypsum is typically less than unity, and therefore gypsum dissolution might also occur in the

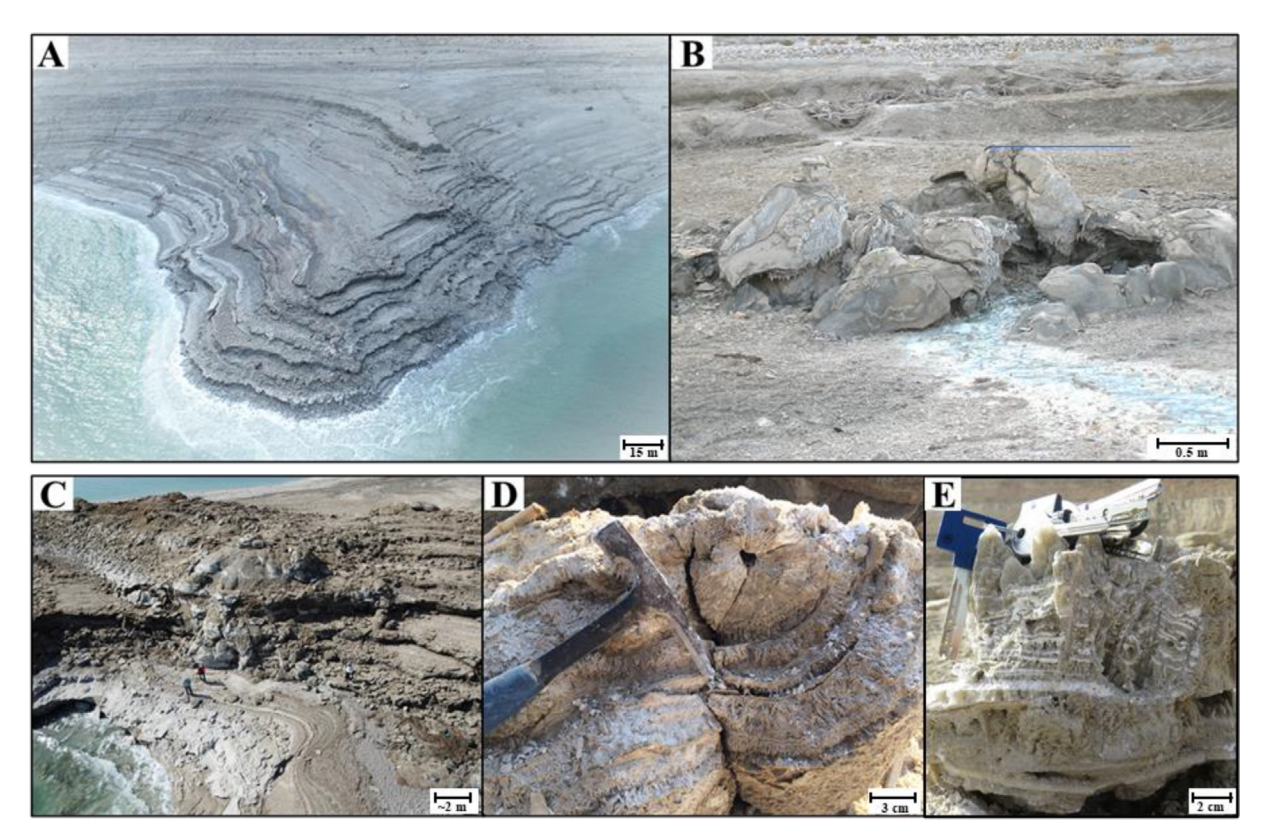


Fig. 2. Field appearances of gypsum structures on the Dead Sea shores: (A) Oblique aerial photo of Cape Qedem "gypsum delta"; (B) A large concentric discordant gypsum structure (one of many) at Ein Qedem shore with a saline spring discharging from it. This suggests that the structures are located at past orifices of groundwater preferential flow paths; (C) Massive cliff-building gypsum cape at Tmarim shore (Cape Tmarim) showing a large discordant gypsum structure (just above the two persons in the lower left), which covers part of this cliff; (D) concentric massive, bladed gypsum that grew around a tree branch (Tmarim shore); (E) large bladed gypsum crystals, about 10 cm long.

subsurface (Gavrieli et al., 2001; Weber et al., 2018) and may have been maintaining the SO_4^{2-} concentrations in the groundwater despite BSR.

3. METHODS

3.1. Study site

The rapid man-made drop of the Dead Sea level, which occurred during the past 4 decades, exposed the sedimentary sequences deposited during the Holocene around the lake. At Ein Qedem and Tmarim shores (Fig. 1), prominent gypsum "capes" termed Cape Qedem (Fig. 2A) and Cape Tmarim (Fig. 2C) have been exposed. These capes comprise the two gypsum facies described in Section 1 above: 1. stratigraphically concordant massive gypsum units with layers containing large bladed crystals and multiple aragonite laminae within or interchanging with the gypsum (Fig. 2); and 2. large discordant gypsum "mound-like" structures containing fine concentric layering (Fig. 2C). The stratigraphically concordant gypsum deposits overlay an erosional unconformity that cut through the last glacial Lisan Formation and are significantly different from the common gypsum deposits in the Dead Sea Formations (e.g., that appear in the Lisan and Ze'elim Formations). The isolated massive discordant gypsum structures are also spread over other shores sites associated with onshore or offshore discharge of saline springs along the Dead Sea western shores (Figs. 1, 2B, C, detailed geological description and radiocarbon dating of the stratigraphic and isolated (discordant) gypsum units see in Weber et al., 2021). The association between the springs system and the massive gypsum structures and mounds suggests that their formation was related to the activity of the saline springs. The location and the shape of these prominent gypsum structures (e.g, Fig. 2B, C) suggest that they were formed around or close to the orifice of ancient springs and hence, carry important information on the hydrological and geochemical histories of the spring-lake system (Weber et al., 2021).

3.2. Sampling

Sediment samples for radiocarbon and C, O, S isotopic analyses were collected in several locations along the retreating shores of the modern Dead Sea, at Ein Qedem and Tmarim shores, where unique gypsum structures (termed gypsum capes) that dissect the typical sedimentary sequences of the Holocene Ze'elim Formation and isolated gypsum mounds are revealed (Fig. 2). The fieldwork included a sampling of "Cape Qedem" and "Cape Tmarim" (Fig. 1B) and gypsum mounds pitted along the Qedem, Samar, Tmarim, and Zuqim shores (Fig. 1A).

3.3. Radiocarbon measurements on aragonite

Radiocarbon ages were determined for calcium carbonate material contained within the concentric gypsum layers (Fig. 2B, D and see Weber et al., 2020). This calcium carbonate consists mainly of the mineral aragonite that precipitated with the gypsum and thus provides additional information on the source of the precipitating solutions. Thirty-five bulk gypsum samples were collected from four sites along the Dead Sea shores (presented in Table 2): 15 samples from Oedem shore. 8 samples from Samar shore. 10 samples from Cape Tmarim, and 2 samples from Zugim shore (Fig. 1). The radiocarbon measurements were conducted at "The National Ocean Sciences Accelerator Mass Spectrometry" (NOSAMS), Woods Hole. The analytical setup included a gas-accepting ion source, connected to a continuous-flow Accelerator Mass Spectrometry (AMS) system, which enabled a rapid direct ¹⁴C measurement on CO₂ gas without the need to convert it to sputtered graphite target (Roberts et al., 2013). Before the analysis, the bulk gypsum samples were ground to powder, and the relative amounts of the mineral phases: gypsum, aragonite, and calcite, were determined by X-Ray diffraction (XRD, Table 2). The carbonate content was also estimated using a "Carbonate Bomb" (computerized and modified version of the "Karbonat-Bombe" of Müller and Gastner, 1971). Then, targeting to have 3 mg of C, the bulk powder was weighted and reacted overnight with H₃PO₄ that released the CO₂ gas directly into a gas-accepting ion source connected to the continuous-flow AMS system at NOSAMS (Roberts et al., 2013). Note that the rapid carbonate ¹⁴C measurements are less precise than the typical radiocarbon measurements sputtered graphite targets. The gas ion source was utilized because it allowed rapid and inexpensive reconnaissance measurements on many gypsum-carbonate mixtures. The measured radiocarbon age for primary aragonite was corrected by the aragonite/calcite ratio as determined by the XRD analyses assuming that the ¹⁴C content of the detrital calcite is zero (e.g., Bookman et al., 2007). The uncertainty in the XRD determination of the aragonite/calcite ratio is equivalent to an age uncertainty of $\sim \pm 150$ yr, interfering with the estimate of the deposition age but not with the "reservoir age", which in turn contains information on the source of radiocarbon (e.g., Stein et al., 2013). The chronology of the "Cape Qedem" structure (along several transects) and the isolated gypsum mounds was determined by radiocarbon dating of terrestrial organic debris collected from the sediments (Weber et al., 2020, 2021).

3.4. Analyses of sulfur and oxygen stable isotopes in gypsum

The sulfur and oxygen isotopic compositions of the sulfate in the gypsum samples, $\delta^{34}S_{gyp}$ and $\delta^{18}O_{gyp}$ were measured at the Godwin Laboratory of the University of Cambridge. These variables are reported as follows:

1.
$$\delta^{34}S_{gyp} = \left(\frac{\left(\frac{34}{32g}\right)_{sample} - \left(\frac{34}{32g}\right)_{std}}{\left(\frac{34g}{32g}\right)_{std}}\right) \times 1000$$
 is the per mil variation from the Vienna Canyon Diablo Troilite (VCDT)

Chemical composition (in molality), stable isotopes and radiocarbon data of the Dead Sea and Ein Qedem brines

	$ m Na^+$	\mathbf{K}_{+}^{+}	$\mathrm{Na^+}$ $\mathrm{K^+}$ $\mathrm{Ca^{2+}}$ $\mathrm{Mg^{2+}}$ $\mathrm{Sr^{2+}}$	${ m Mg}^{2+}$	Sr^{2+}	 []	Br^-	$Cl^ Br^ SO_4^2$ H_2S	H_2S	TDS	TDS Density $\delta^{34}S_{SO4}$	δ^{34} Sso4	$\delta^{34} S_{H2S}$	δ^{18} Oso4	DIC	14 C
	mol·kg	$mol \cdot kg H_2O^{-1}$								$g.L^{-1}$	$g \cdot L^{-1}$ $kg \cdot L^{-1}$	%0	%00	0%	mol·m ⁻³ fmc	fmc
Dead Sea	1.53	0.227	1.53 0.227 0.525 2.17 0.0046 7.26 0.071 0.0046	2.17	0.0046	7.26	0.071	0.0046	0	348	1.24	14.1	-17*	11.4	1.0	0.75
Ein Qedem 1.21 0.11 0.319 0.91 0.0026 3.72 0.034 0.0092 0.0015	1.21	0.11	0.319	0.91	0.0026	3.72	0.034	0.0092	0.0015	190	1.13		24.5 ± 0.85 -12.1 ± 0.56 16.2 ± 0.71	16.2 ± 0.71	3.3	0.08
Dead Sea dat	a sources:	major ions	s concentra the overtu	tion (2008	3) from Rez	mik et al.	, 2009b, L	OIC (2013)	from Golar	i et al., 20]	16; $\delta^{34}S_{SO4}$;	and $\delta^{18}O_{SO4}$ (20) and $\delta^{14}C$ from Tab	Dead Sea data sources: major ions concentration (2008) from Reznik et al., 2009b, DIC (2013) from Golan et al., 2016; $\delta^{34}S_{SO4}$ and $\delta^{18}O_{SO4}$ (2013) from Levy et al., 2019, $\delta^{34}S_{H2S}$ is the value from the Dead Sea hynoliumion before the overturn when the hottom water hody was anoxic the corresponding $\delta^{34}S_{SO4}$ was 14 5%, $\delta^{14}C$ from Talma et al. 1997. Fin Dedem data sources: major ions	al., 2019, δ^{34} S in Oedem data	H2S is the valu	e from
DIC and 14C	from Web	er et al., 20	118. The sta	able isotor	ses were me	asureda	s part of t	his study or	n groundwa	iter sampl	es from Ein	Qedem springs	DIC and ¹⁴ C from Weber et al., 2018. The stable isotopes were measured as part of this study on groundwater samples from Ein Qedem springs (2018) applying the same procedure as that used for	the same proce	dure as that u	sed for
the gypsum s.	amples after pr	ter precipit	ating BaSC	O ₄ and Zn	S from the	water sa	3 mples: δ^3	⁴ S _{SO4} (ave	age of 15 s	amples), à	3 ³⁴ S _{H2S} (ave	erage of 12 sam	the gypsum samples after precipitating BaSO ₄ and ZnS from the water samples: $\delta^{34}S_{SO4}$ (average of 15 samples), $\delta^{34}S_{H2S}$ (average of 12 samples) and $\delta^{18}O_{SO4}$ (average of 5 samples), the error	et (average of :	samples), th	e error

range is one standard deviation.
* An historical value for the lake's anoxic hypolimnion (with evidence of BSR, conditions not prevailing today in the Dead Sea), before the lake's overturn in 1979 (Nissenbaum and Kaplan, * An historical value for the lake's anoxic hypolimnion (with evidence of BSR, conditions not prevailing today in the Dead Sea), before the lake's overturn in 1979 (Nissenbaum and Kaplan,

Table 2 XRD, stable isotopes and radiocarbon data of the bulk gypsum samples.

Sample ID	Site	Elevation	XRD re	sults ^b								%	Aragonite	Gypsum		Aragonite		
		(m bmsl ^a)	gypsum	aragonite	calcite	halite	quartz	Bischofite	Carnallite	Iron oxide	Other	CaCO ₃ ^c	fraction in CaCO ₃ ^d	δ ³⁴ S _{SO4} (‰)	δ ¹⁸ O _{SO4} (‰)	Measured 14C age (y)e	±	Corrected ¹⁴ C age (y)
NWG-12	Tmarim	420	86	12	2		1						0.86	16.1				
NWG-13	Tmarim	420	90	10									1.00	16.1				
NWG-14	Tmarim	425	94	3		1	1			1		5.7	1.00	16.2		6940	140	6940
NWG-15	Tmarim	425	68	10	1	13	7					13.3	0.91	15.9		6050	145	5290
NWG-16	Tmarim	425	88	3	1	5	1			1			0.75	15.8	14.8			
NWG-17	Tmarim	425	86	5		9							1.00	15.6				
NWG-18	Tmarim	425	99	1								1.5	1.00	15.5		5800	140	5800
NWG-19	Tmarim	425	94	2		3	1						1.00	15.0	15.7			
NWG-20	Tmarim	425	91	4		5						2.4	1.00	15.2		5510	130	5510
NWG-21	Tmarim	425	80	10		8	1					17.8	1.00	16.1		4610	125	4610
NWG-22	Tmarim	425	98	2								2.3	1.00	15.6	16.2	4870	120	4870
NWG-23	Tmarim		45	36			1	10			8	43.8	1.00	14.8		3560	110	3560
NWG-24	Tmarim		100									1.6	1.00	15.0		7370	150	7370
NWG-25	Tmarim	425	92	4	3	1							0.57	14.8				
NWG-26	Tmarim	420	89	10			1					17.0	1.00	16.0	14.9	4010	125	4010
NWG-27	Tmarim	418.6	99	1								1.2	1.00	14.8	15.3	3980	135	3980
NWG-28	Tmarim	418.6	90	1			5				5		1.00	14.9				
NWG-29	Zuqim	414.6	81	18	1							33.5	0.95	15.8	14.7	3240	120	2810
NWG-30	Zuqim	419.6	65	16	1	16	1					20.2	0.94	15.8	15.2	3580	125	3090
NWG-31	Qedem	419.7	88	7	2	1	2					11.3	0.78	16.1	15.7	6450	130	4430
NWG-32	Qedem	419.7	86	8	2	1	3					11.8	0.80	14.1	14.7	7090	130	5300
NWG-33	Qedem	416.5	76	8	7	2	2		5			11.0	0.53	15.7	14.9	, 0, 0	100	2200
NWG-34	Qedem	419.1	92	6	1	_	1		, and the second			12.6	0.86	16.9	1	9070	155	7830
NWG-35	Qedem	418.6	92	3	2	2	1					12.0	0.60	14.6		,,,,	100	, 020
NWG-36	Oedem	420.2	85	11	_	2	1		1			12.7	1.00	16.8	15.1	8240	155	8240
NWG-37	Qedem	420.2	76	13		10	1		•			17.2	1.00	15.6	14.9	6010	135	6010
NWG-38	Qedem	420.2	76	14	3	7	-					16.3	0.82	15.8	14.6	6630	135	5070
NWG-39	Qedem	420.2	84	12	_	•	3					14.7	1.00	15.8		5610	135	5610
NWG-40	Qedem	423.8	19	81								61.6	1.00	10.0		2870	105	2870
NWG-41	Qedem	423.8	93	2	2	2	2					4.9	0.50	15.9	15.8	9680	165	4110
NWG-42	Qedem	422.8	95	4	-	~	2					6.1	1.00	16.0	15.0	6350	135	6350
NWG-43	Qedem	422.8	94	3		2	1					4.1	1.00	15.7	15.4	6080	130	6080
NWG-44	Qedem	422.8	91	3	2	2	3					5.3	0.60	15.0	16	7460	155	3350
NWG-45	Qedem	424.2	97	2	_	_	1					3.7	1.00	16.2	10	15,980	325	15,980
NWG-46	Qedem	424.2	67	10	2	8	1		11			11.7	0.83	14.6		7050	140	5580
NWG-40	Qedem	424.2	95	4	_	J	1		11			11.7	1.00	16.6	15.1	12,940	240	12,940
NWG-48	Samar	424.1	97	3			1					2.7	1.00	16.5	16.2	11,620	215	11,620
NWG-49	Samar	424.1	79	9	1	2			8			14.8	0.90	15.8	10.2	6380	140	5530
NWG-49	Samar	420.8	87	9	1	1	1		U			12.0	0.90	15.3		7290	150	6450
NWG-50 NWG-51	Samar	420.8	94	3	1	2	1					7.6	0.75	15.5	15.8	8140	150	5830

VWG-52	Samar	418.7	85	13			2	18.4	1.00	15.0		6190	135	6190
VWG-53	Samar	418.3	06	4	7	7	2	6.6	0.67	14.8	15	8850	170	5590
VWG-54	Samar	414.1	68	=				21.4	1.00	15.9		4430	120	4430
VWG-55	Samar	412.9	93	3	7	1	2	11.6	09.0	15.8	15.3	7120	145	3020
a Mater be	lare halow manne and reta	level level												•

XRD (X-ray diffraction) results are based on the patterns reference intensity ratio (RIR), assuming no preferred orientation and no amorphous phases in the sample.

the carbonate content estimated using a "Carbonate Bomb"

the ratio of aragonite to calcite + aragonite based on the XRD estimate. Rapid radiocarbon analysis of aragonite was measured at the AMS NOSAMS facilities with standard error.

Corrected ¹⁴C age of the aragonite was calculated from the aragonite fraction in the sample's CaCO₃ content according to Eq. 6 of Bookman et al. (2007)

standard; and 2. $\delta^{18}O_{gyp}$, which has a similar equation as $\delta^{18} O_{gyp}$ (but the ratios $\frac{^{34}S}{^{32}S}$ substitute by $\frac{^{18}O}{^{16}O}$) and scaled to the Vienna Standard Mean Ocean Water (VSMOW) standard. Gypsum samples were dissolved with double deionized water, and the resulting sulfate was re-precipitated as barite (BaSO₄) by adding saturated barium chloride (BaCl₂) solution and then left overnight for barite to recrystallize and fully precipitate. The barite was subsequently filtered out of solution, rinsed with HCl acid (6N) and deionized water, and dried at 50°C in an oven. The barite precipitate was pyrolyzed at 1450°C in a Temperature Conversion Element Analyzer (TC/EA), and the resulting carbon monoxide (CO) was measured by continuous flow GS-IRMS (Gas Chromatography-Isotope-ratio mass spectrometry) (Thermo, Delta V Plus) for its $\delta^{18}O_{SO_4}$. For the $\delta^{34}S_{SO_4}$ analyses, either barite or the original gypsum was combusted at 1030°C in a Flash Element Analyzer (EA), and the resulting sulfur dioxide (SO₂) was measured with continuous flow GS-IRMS (Thermo, Delta V Plus). Samples for $\delta^{18}O_{SO_4}$ were measured in replicates (3 times, or more when the difference exceeded 0.8%), and the standard deviation of analyses was used as the external reported error ($\sim \pm 0.5\%$). The $\delta^{18} O_{SO_4}$ values are reported vs. VSMOW and were corrected to the known values of two barite standards, NBS 127 and EM barite having $\delta^{18}O_{SO_4}$ values of 8.6% and 15%, respectively. These standards were run at the beginning and end of each set of 8-12 samples. $\delta^{34}S_{SO_4}$ values are reported vs. VCDT standard and were corrected to the known values of NBS 127 and EM barite standards with $\delta^{34}S_{SO_4}$ values of 20.3% and 12%, respectively. The error was determined from the standard deviations of NBS 127 standard at the beginning and the end of each set ($\sim \pm 0.4\%$).

3.5. Thermodynamic calculations

The reaction for gypsum dissolution and precipitation is given by:

$$CaSO_4 \cdot 2H_2O \leftrightarrow Ca^{2+} + SO_4^{2-} + 2H_2O$$
 (1)

The degrees of saturation (Ω) with respect to gypsum and gypsum precipitation potential (PPt) were calculated using the Pitzer thermodynamic database (pitzer.dat) in PHREEQC software (v. 2.18.5570, Parkhurst and Appelo, 1999).

The equation defines Ω as:

$$\Omega = \frac{IAP}{K_{sp}} = \frac{a_{Ca^{2+}} \cdot a_{SO_4^{2-}} \cdot a_{H_2O}^2}{\left(a_{Ca^{2+}} \cdot a_{SO_4^{2-}} \cdot a_{H_2O}^2\right)_{eq}}$$
(2)

where IAP and K_{sp} are the ions activity product and the thermodynamic solubility product (the activity product at saturation), respectively. a_i is the activity of the species i and the subscript eq denotes equilibrium.

PPt is defined as the amount of gypsum that should precipitate from supersaturated solution (i.e., $\Omega > 1$) to attain equilibrium (saturation, $\Omega = 1$). In the case of Ca-chloride solutions (i.e., $[Ca^{2+}]\gg[SO_4^{2-}]$) PPt is expressed by the equation:

$$PPt = [SO_4^{2-}]_{sample} - [SO_4^{2-}]_{sat}$$
(3)

where $[SO_4^{2-}]_{sample}$ and $[SO_4^{2-}]_{sat}$ are the sulfate concentrations (in molality units) in the sample and at saturation with respect to gypsum, respectively.

4. RESULTS

4.1. Radiocarbon ages of the authigenic aragonite

Radiocarbon ages of the authigenic aragonite from the discordant gypsum structures provide calibrated ages in the range of 2800 and 16,000 cal yr BP (Table 2, the correction is only for calcite content). These ages are significantly older than the radiocarbon ages of the organic debris collected from the same gypsum units.

4.2. $\delta^{34}S_{SO_4}$ and $\delta^{18}O_{SO_4}$ of the gypsum

Both sulfur and oxygen isotopic compositions of the sulfate in the gypsum from Cape Qedem and the gypsum mounds (discordant gypsum) at Ein Qedem shore and the other locations along the Dead Sea shores lie in narrow ranges (Fig. 3). Sixty-eight $\delta^{34}S_{gyp}$ samples of gypsum from

different types and locations lie between 14.1% to 16.9% with an average of $15.8\pm1\%$ and 31 samples of $\delta^{18}O_{gyp}$ lie between 14.4% to 16.5% with an average of $15.3\pm0.6\%$. The uniformity in these isotopic compositions (Fig. 3D) suggests a uniform source for the precipitating solutions. It should be noted that the sulfur and oxygen isotopic compositions of gypsum are similar to the values expected for gypsum that precipitated from the Dead Sea brine itself (Table 1), taking into account mass-dependent isotopic fractionation values ($\Delta = \delta_{soild}$ - $\delta_{solution}$) of 2% and 3.3% for sulfur and oxygen isotopes, respectively (van Driessche et al., 2016, Fig. 3A, black and yellow crosses).

5. DISCUSSION

5.1. the role of the saline springs in near shore gypsum precipitation

The Ein Qedem and the Dead Sea are both Ca-chloride brines that evolved from the ancient marine-derived brine of the Sedom lagoon that filled the basin during the late Neogene. This ancient Sedom brine was modified later by mixing with freshwater and deposition of primary minerals (Stein et al., 1997; Starinsky and Katz, 2014; Stein, 2014

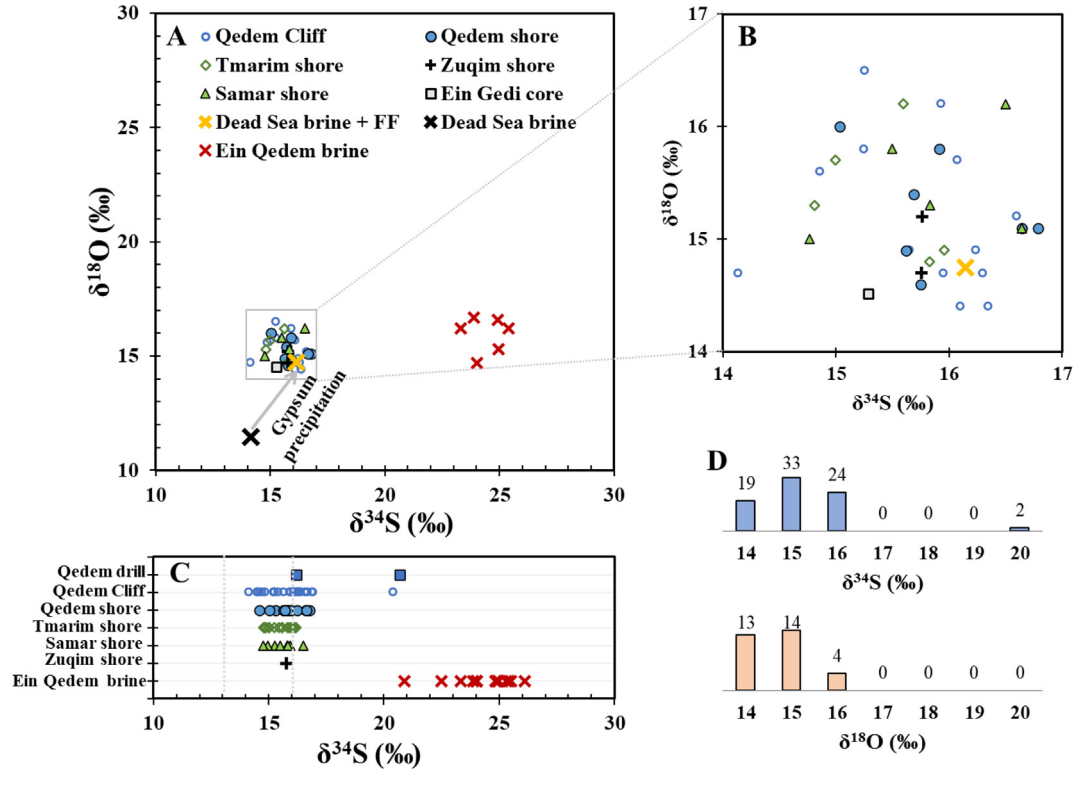


Fig. 3. $\delta^{34}S$ and $\delta^{18}O$ of SO_4^{2-} in gypsum and waters from various locations along the Dead Sea shore (see map in Fig. 1). (A) $\delta^{34}S$ vs. $\delta^{18}O$ of the gypsum's SO_4^{2-} . Legend: black cross - Dead Sea sulfate in 2013 (Levy et al., 2019, Table 1); yellow cross: the calculated isotopic composition of gypsum precipitating from Dead Sea brine assuming isotopic fractionations between solid and brine of 2% for $\delta^{34}S$ and 3.3% for $\delta^{18}O$ (the gray arrow); red crosses: isotopic values of Ein Qedem brine; empty squares: gypsum from Ein Gedi core (data from Torfstein and Turchyn, 2017). (B) Zoom into the gray square in (A). (C) $\delta^{34}S$ values of all gypsum samples and Ein Qedem brine from this study sorted by location (vertical axis). Not all samples are plotted in (A) due to lack of $\delta^{18}O$ data. The additional lower $\delta^{34}S$ value for Ein Qedem brine (red cross) was sampled in 1996 (from Gavrieli et al., 2001). (D) Histogram of $\delta^{34}S$ and $\delta^{18}O$ in the various gypsum samples. The standard deviation for $\delta^{34}S$ is $\pm 0.5\%$ and for $\delta^{18}O$ is $\pm 0.4\%$.

and references therein). Yet, several significant differences distinguish the Ein Qedem and the modern Dead Sea brine (e.g., Fig., 3, Table 1). The former is a more dilute solution (\sim 190 g·L⁻¹ vs. \sim 350 g·L⁻¹ total dissolved salts) and have higher Na $^+$ /Cl $^-$ ratio (\sim 0.3 vs. \sim 0.2). Based on geochemical similarities to porewater extracted from the Dead Sea drilled core and the radiocarbon and radiokrypton ages, Weber et al. (2018) suggested that the Ein Qedem saline springs discharge the solution that was part of the epilimnion of the last glacial Lake Lisan, the precursor of the Holocene Dead Sea. The significantly more saline Dead Sea brine has since evolved through major evaporation, salt precipitation, and lake-overturning events (Steinhorn et al., 1979; Levy et al., 2018). Radiocarbon content in the Ein Qedem brine is very low, ~ 0.075 fMC (fraction of modern carbon units), reflecting its origin from the last glacial Lake Lisan and long isolation time in the regional aquifers (Weber et al., 2018). On the other hand, the Dead Sea, which receives flood-water with high radiocarbon content (due to rapid exchange with the atmosphere, Belmaker et al., 2007), have retained relatively high radiocarbon values during the Holocene (\sim 0.75 to 0.85 fMC, Talma et al., 1997).

Radiocarbon dating of the aragonite interbedded within the gypsum structures (after correction for the aragonite/calcite ratio in the carbonate sediments), yields apparent ages that in most cases are older than the calendar ages of the structures' deposition. The apparent ages termed here "aragonite ages" are the ¹⁴C age of the aragonite as calculated from its measured ¹⁴C content. The calendar ages are determined by radiocarbon dating of organic debris recovered from the structures (termed here as t_{real}, the "real" ¹⁴C age of organic debris sampled from the same horizon as the aragonite, the yellow circles in Fig. 4A). All samples of organic debris yielded (calibrated calendar) ages that lie at the late Holocene time interval (past ~4000 y, Weber et al., 2021). Accordingly, we assume (as a null hypothesis) that all gypsum structures (even those without organic debris suitable for radiocarbon dating) located at similar elevations along the retreating shores of the modern Dead Sea (shown in Fig. 1) were formed during the past 4000 y.

The older "aragonite ages" probably reflect the contribution of DIC (dissolved inorganic carbon) with low ¹⁴C content from the "old" Ein Qedem Ca-chloride brine (see above) to the precipitation of the authigenic aragonite. Assuming that the individual gypsum structures were deposited during a short time interval, we can calculate the contribution of the DIC from the saline springs (f_{EO}) to the structure (see Appendix A for explanation). As an example we estimate here the f_{EO} of the concentric layers of a discordant gypsum structure, ~4 m in diameter (Fig. 4B). In order to calculate the f_{EO} in the different concentric layers of a gypsum structure (e.g., samples 1-4 in Fig. 4B), we need the "real" age (t_{real}) of the structure and t_{app} , the apparent (and older) ^{14}C age of the aragonite as a result of adding low ¹⁴C from Ein Qedem brine (see the relation between t_{real} and t_{app} in Fig. 4A). However, we usually measured t_{app} because the abundance of organic debris within the gypsum structure is low. Hence, we attempted to

estimate the possible range of treal of the concentric gypsum structures from the lake level curve (Weber et al., 2021). Assuming that the structure was formed around the brine's discharge orifice very close to the lake level of that time, we picked from the lake level curve the times (to represent t_{real}) when the level was at the structure's elevation (\sim 420 m bmsl). The youngest time was 700 yr cal BP, the last time that the lake level was at that elevation and 2900 yr BP, which was the previous prolonged significant lake level drop to this elevation. Calculating f_{EO} with these estimates of t_{real} and the measured t_{app} for the gypsum structure depicted in Fig. 4B, yielded f_{EQ} estimates of 0.26 to 0.9 for $t_{real} = 700$ yr cal BP (blue fonts in Fig. 4B) and 0.14 to 0 for $t_{real} = 2900$ yr cal BP (purple fonts in Fig. 4B). These results (Fig. 4B) suggest that Ein Oedem brine contributed more DIC during the beginning of structure's formation (close to its center). A contribution of Ein Oedem brine to aragonite formation is evident from the radiocarbon ages of the aragonite. Considering the process of co-precipitation of the minerals aragonite and gypsum, the ancient springs of Ein Qedem had an important role in creating the gypsum structures.

5.2. Mechanisms of gypsum formation

While the radiocarbon content of aragonite indicates a potential contribution of the Ein Qedem brine to the formation of the gypsum structures, gypsum is currently not precipitating in the area where the Dead Sea and the Ein Qedem brines mix. Moreover, the values of the $\delta^{18}O$ and $\delta^{34}S$ in the gypsum structures are similar to the values of gypsum that would be formed from the modern Dead Sea brine solely, with no contribution of sulfate from the Ein Qedem brine (Fig. 3). This apparent discrepancy can be addressed by considering the thermodynamic and kinetic conditions for gypsum precipitation from the Dead Sea brine and the geochemical evolution of the Dead Sea and the Ein Qedem brines.

5.2.1. Thermodynamics and kinetics of gypsum precipitation in the Dead Sea

The modern Dead Sea is supersaturated with respect to gypsum ($\Omega = 1.42$ in 2008). Reznik et al. (2009b) argue that the Dead Sea brine retains high degree of supersaturation due slow kinetics of gypsum nucleation and crystal growth as compared to other natural solutions with similar degrees of supersaturation. They attributed the slow kinetics in the Dead Sea to the low gypsum solubility, which at the extremely high Ca^{2+}/SO_4^{2-} ratio of the Dead Sea (~115) and its high ionic strength is controlled by SO_4^{2-} variations (Fig. 5). In addition, the inhibitory effect of Na⁺ also reduces the rate of crystal growth. Finally, lack of crystallization surfaces prevents crystal growth from taking place, thereby forcing the system to be limited by the rate of nucleation and suspension time of the crystals in the brine, which together enable the long-term supersaturation of the brine (Reznik et al., 2009b). Even higher gypsum supersaturation has been reported for the less saline hypolimnetic brine of Lake Lisan (Levy et al., 2019).

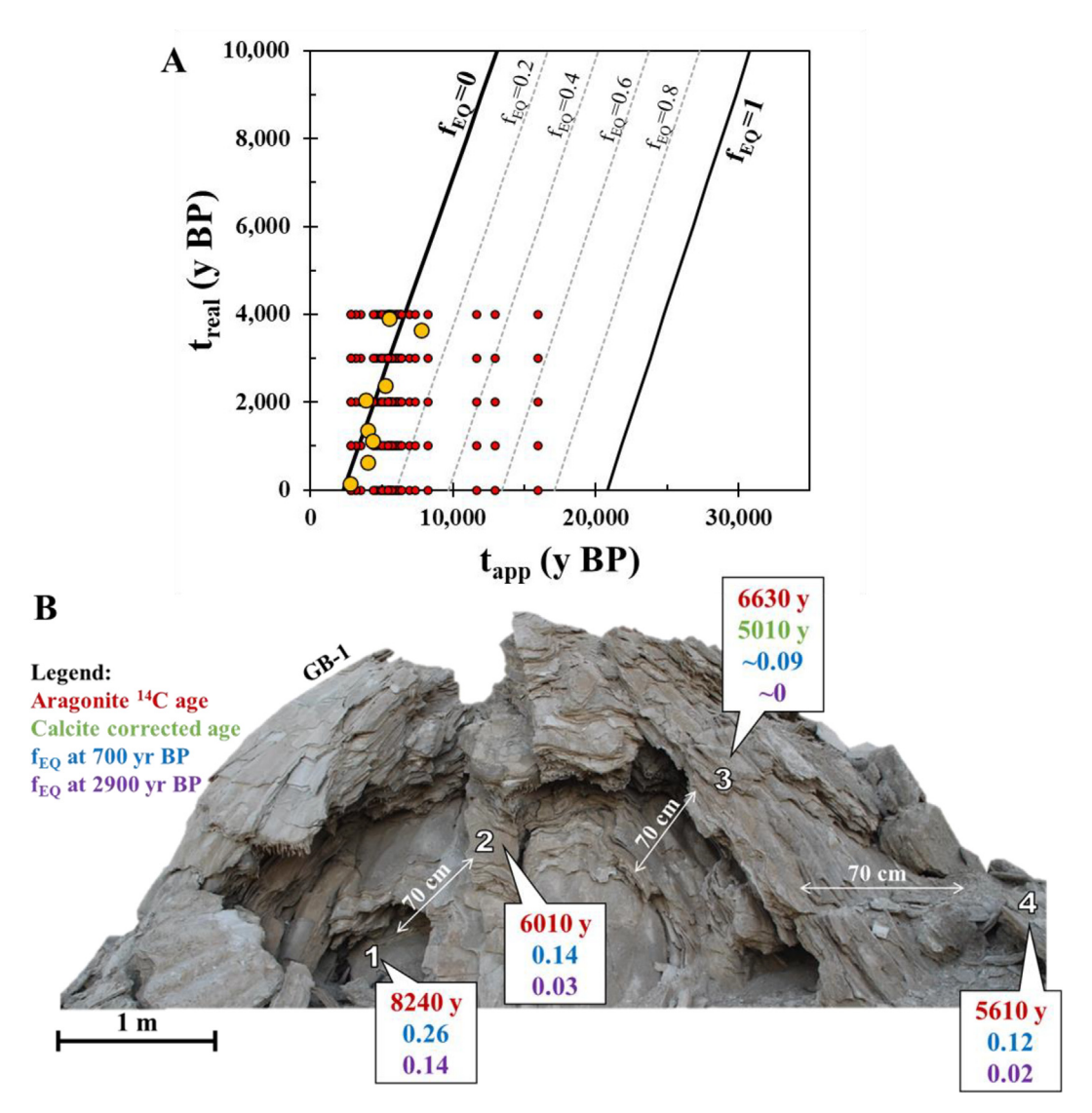


Fig. 4. Radiocarbon ages of aragonite within gypsum. (A) tapp (apparent aragonite ages) versus treal (real ages of organic debris); Six straight lines of constant f_{EO} (fraction of Ein Qedem brine in a weight mixture of Ein Qedem with Dead Sea brines, f_{EO}=0 denotes zero contribution of "old" Ein Qedem brine meaning pure Dead Sea brine) values from f_{EQ} =0 to f_{EQ} =1 are plotted according to a modified linear equation of Weber et al. (2020), in which the intercept contains an expression for f_{EQ} (see appendix for the equation and its explanation). The solid yellow circles are the samples on which both, treal and tapp were measured, while for the red circles have only tapp. The solid red circles represent the t_{app} ages for samples on which t_{real} was not determined. These samples were plotted on arbitrarily guessed t_{real} ages (in time intervals of 1000 yr) between 0 to 4000 yr BP. Samples that plot well to the left of the line for f_{EQ}=0 (forbidden zone according to the linear equation of Weber et al., 2020) indicate that their real age is younger than their guessed treal age. Note that most of the aragonite sample have rather small fraction of DIC from Ein Qedem brine ($f_{\rm EQ}$ of \sim 0.03 or 3% as indicated by the best fit of the yellow solid circles). However, the three rightmost aragonite samples (red solid circles) show significant contribution of Ein Qedem's DIC in their aragonite (f_{EO} between 0.4–0.5 or 40-50%). (B) Radiocarbon ages and f_{EQ} in four concentric layers (marked as samples 1-4) of one of the discordant gypsum bodies which were formed around the orifice of Ein Qedem brine discharge by mixing of this brine with Dead Sea brine (see text and Weber et al., 2021) and are currently exposed on the Qedem shore. Radiocarbon ages of pristine aragonite are presented in red fonts; sample number 3 was a mixture of aragonite and calcite, and its corrected age (for the calcite content) is presented in green fonts. f_{EO} for each of the four layers was estimated from its ¹⁴C content and its age, assuming that the whole structure was formed during very short period (several decades up to 100 yr.) at the age of: 1. 700 yr BP, which was the last time (before present) that the lake level was at the elevation of this gypsum body and hence the Ein Qedem brine orifice could have been active (blue fonts); and 2. 2900 yr BP, which was the previous prolonged significant lake level drop (purple fonts).

5.2.2. Dead Sea-Ein Qedem mixtures

The Ein Qedem brine is undersaturated with respect to gypsum ($\Omega=0.7$, Fig. 5) and evidence for some gypsum dissolution by the Qedem brine during its ascent from

depth (and mixing with Dead Sea brine) was reported by Weber et al. (2018). Observations on the Dead Sea shores did not reveal any gypsum precipitation at the sites where Ein Qedem springs mixes with the Dead Sea brine. This is

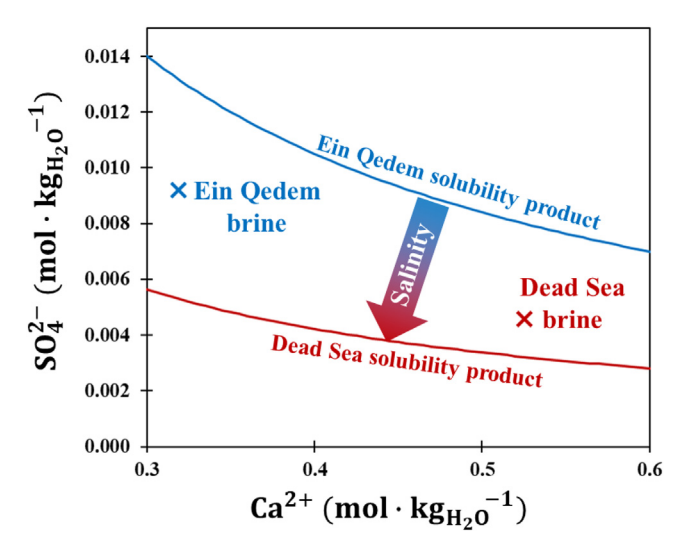


Fig. 5. Solubility product curves of gypsum for Ein Qedem and Dead Sea brines (calculated using PHREEQC, v. 2.18.5570, Parkhurst and Appelo, 1999). plotted on SO_4^{2-} vs. Ca^{2+} field and the composition of Ein Qedem (blue cross) and the Dead Sea (red cross) brines. Note that the scale of the y-axis is 100 times smaller than the x-axis, the solubility decreases with increasing salinity and Ein Qedem brine is undersaturated with respect to gypsum (lies below its solubility curve), while Dead Sea brine is supersaturated (lies above its solubility curve).

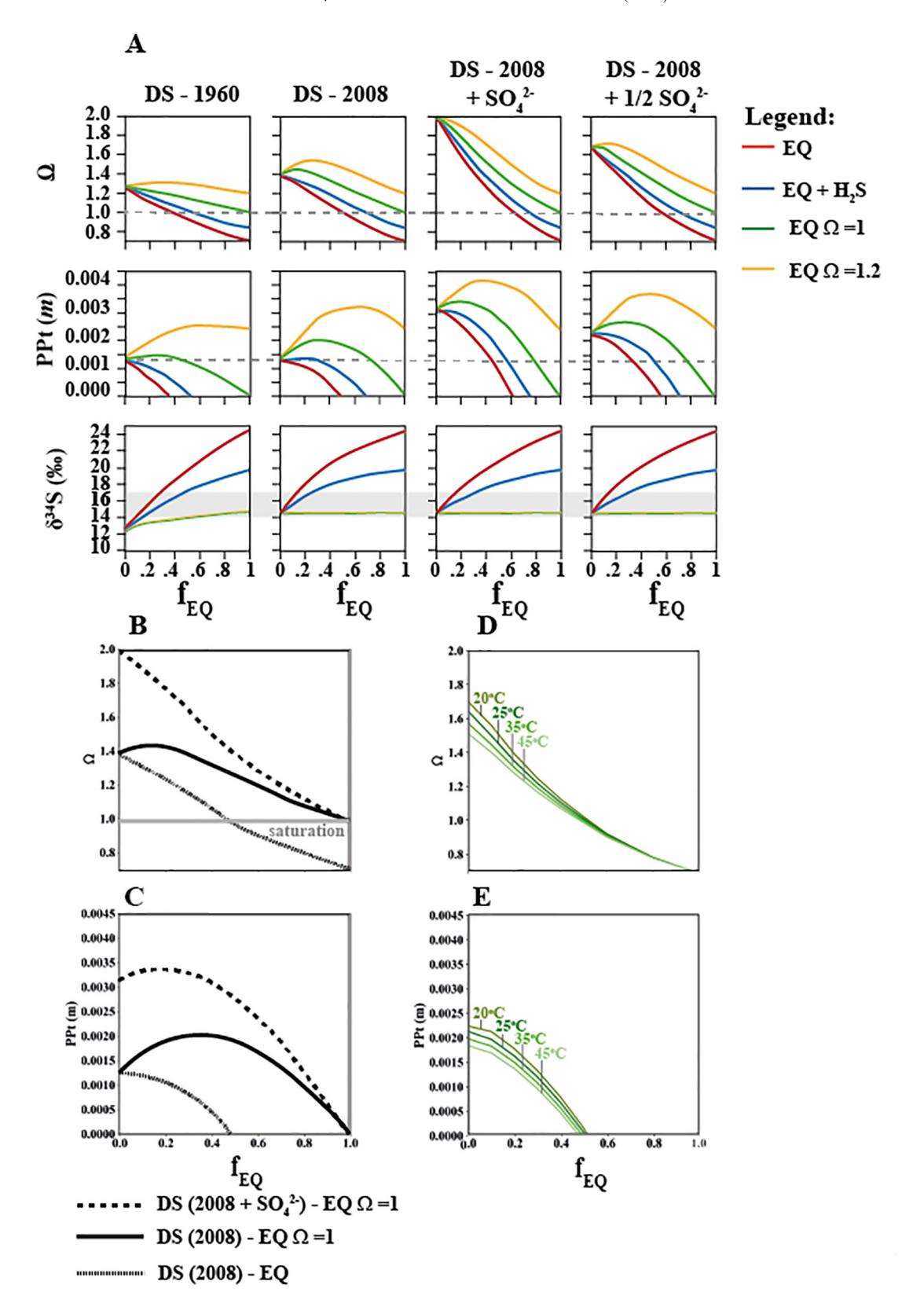
despite the higher concentration of sulfate in the Ein Qedem saline springs (Table 1). Finally, thermodynamic calculations show that the degree of saturation with respect to gypsum of Dead Sea-Ein Qedem mixtures is lower than the Ω and PPt of the Dead Sea itself, confirming our observations (Fig. 6). This indicates that in order to induce gypsum deposition from Dead Sea-Ein Qedem mixtures, as occurred 6600–600 years ago at the Qedem area, SO_4^{2-} concentration in the mixture must had been higher. Hereafter we provide evidence that the concentration of sulfate in Ein Qedem and Dead Sea was higher than at present and run mixing models to examine potential mixing compositions between the past Dead Sea and past Ein Qedem. The models show the feasibility for Dead Sea-Ein Qedem mixtures to form the observed Qedem and Tmarim gypsum capes and the other gypsum structures discussed above and their isotopic compositions.

5.2.3. Evolution of Ein Qedem in the subsurface

We first examine the possibility that SO_4^{2-} concentration in the Ein Oedem type groundwater was higher in the past. As discussed above, the Ein Qedem brine is undersaturated with respect to gypsum ($\Omega = 0.7$), anoxic, and contains high levels of dissolved sulfide (Table 1), indicating that the brine underwent BSR since it was last in contact with gypsum (Gavrieli et al., 2001). BSR in the subsurface is also implied by the rather high $\delta^{34}S_{SO_4}$ of the Ein Qedem brine, which is the result of production of isotopically "light" sulfide by Rayleigh type fractionation. If BSR is an ongoing process occurring in the deep aquifer, it is possible that hundreds and thousands of years ago, the brine contained higher SO_4^{2-} amounts, some of which have been reduced to sulfide over time. According to this scenario, the initial sulfate's sulfur and oxygen isotopic compositions were less enriched (i.e., has lower values), and were enriched (values increased) with time as BSR progressed. The Ω of the Ein Qedem

source water that percolated to the subsurface is unknown. However, if it was the epilimnetic solution of Lake Lisan (Weber et al., 2018), it most likely percolated to the subsurface as gypsum-saturated or supersaturated brine. Indeed, Gavrieli et al. (2001) showed that other saline groundwaters in the Dead Sea Quaternary aguifer are supersaturated with respect to gypsum, such as Einot Zugim 1 ($\Omega = 1.12$) and DSIF well (Wadi Ze'elim) ($\Omega = 1.45$), while Levy et al., (2019) showed that the solution of Lake Lisan hypolimnion (the epilimnion is the mother brine of Ein Qedem, according to Weber et al., 2018) was at times also supersaturated. Thus, it is rather safe to assume that the original Ein Qedem brine (comprising the epilimnion solution of Lake Lisan that ingressed into the regional aquifers) contained higher amount of SO₄²⁻ and was most likely supersaturated with respect to gypsum.

Now, we examine four possible mixing scenarios for Ein Qedem brine solution, each with different SO₄²⁻ concentration (the four colors for the curve in Fig. 6a): (1) The measured Ein Qedem composition; (2) Considering the H₂S in the brine solution (0.002 mol·kg H_2O^{-1}) as oxidized and hence added as SO_4^{2-} to the measured SO_4^{2-} concentration; (3) Gypsum-saturated Ein Qedem brine solution ($\Omega = 1.0$: SO_4^{2-} concentration was increased to attain saturation); and (4) Ein Qedem brine solution at $\Omega = 1.2$. These four solutions were mixed (in all mixing ratios) with four different Dead Sea brines having with different sulfate concentrations (the four columns in Fig. 6A), and the resultant Ω , PPt and $\delta^{34}S_{gyp}$ were calculated (the four rows in Fig. 6A). As expected, the increasing SO_4^{2-} concentrations in the springs increase both Ω and PPt at a given mixing ratio (the 2 columns on the left in Fig. 6A). However, these Ω and PPt are still relatively moderate for gypsum precipitation and will not support massive gypsum sedimentation as seen in the Cape Qedem and the other gypsum structures exposed today along the Dead Sea shores. As discussed



briefly at the top of this section, SO_4^{2-} concentration in the Dead Sea during the time of massive gypsum deposition was also higher than at present. This scenario is evaluated in the following section.

5.2.4. Change in SO_4^{2-} in the Dead Sea during the past century – implications to past changes

During the past seven kyr, the Dead Sea level fluctuated between \sim 380 to \sim 430 m bmsl (Weber et al., 2021). A modern analog for variations in the lake's chemistry as a result of such fluctuations is the Dead Sea composition in the years 1960 and 2008, during which the lake level dropped dramatically (as a result of anthropogenic diversion of freshwater and evaporation in ponds of the potash plants) from 397.5 m bmsl to 421 m bmsl (Israel Water Authority, Reznik et al., 2009b). Under natural conditions gypsum precipitated from the brine during period of lake level drop but likely maintained oversaturation due to the slow nucleation and growth kinetics. However, since the 1960's most of the sulfate that the Dead Sea lost was precipitated as gypsum in the industrial evaporation ponds in the southern shores of the Dead Sea (Reznik et al., 2009b). The intensive evaporation in the industrial ponds increased the Ω beyond the kinetic barrier for nucleation and triggered precipitation of gypsum, ending with extremely low sulfate concentration of 0.001 mol·kg⁻¹ in the brines which returned back to the Dead Sea (Reznik et al., 2009b). In view of this anthropogenic intervention, our models simulations to the natural conditions considered also four scenarios of different SO₄² concentrations in the Dead Sea (the four columns in Fig. 6A, ordered from left to right in and itemized from 1-4): (1) the year 1960 (SO_4^{2-} concentration in the Dead Sea of 0.0050 mol·kg⁻¹), which represents the Dead Sea high lake level; (2) the year 2008 (SO_4^{2-} concentration in the Dead Sea of 0.0033 mol·kg⁻¹), which represents the Dead Sea low lake level; (3) the Dead Sea sulfate during the year 2008 (scenario #2) plus the amount of SO_4^{2-} lost since 1960 by anthropogenically induced gypsum precipitation $(SO_4^{2-}$ concentration in the Dead Sea of 0.0046 mol·kg⁻¹); and (4) same as scenario #3 but adding only 50% of the amount of SO₄²⁻ lost anthropogenically since 1960 (SO₄² concentration in the Dead Sea of $0.0039 \text{ mol} \cdot \text{kg}^{-1}$).

The Dead Sea brine can maintain supersaturation with respect to gypsum over a prolonged period due to its high Ca²⁺/SO₄²⁻ ratio and high ionic strength (Reznik et al., 2009b). Mixing with various Ein Qedem solutions (end members in the calculation, $Ca^{2+}/SO_4^{2-} \sim 21-35$) reduces this ratio and the ionic strength, thereby moving the system towards overcoming the kinetic barrier to precipitation. Hence, these mixtures may precipitate more gypsum even when their Ω is close to that of the Dead Sea. However, a significant increase in the Ω relative to the Dead Sea end member (Fig. 6A) is obtained only in the two scenarios in which the saturated Ein Oedem brine was mixed with Dead Sea brine of 2008 (as in scenario #2) enhanced with 100% and 50% of the amount of SO_4^{2-} lost in the industrial evaporation pans since 1960 (scenarios #3 and #4 above, respectively). In these scenarios, there is a clear preference for gypsum precipitation from the mixtures. Yet, the fact that in all other mixtures, Ω is not much higher than that of the Dead Sea is not in itself evidence that these conditions did not favor gypsum precipitation. In all the mixtures of Dead Sea brine from 2008 (including the added SO_4^{2-}) and the sulfate-enriched Ein Qedem brines, the PPt curve forms a peak, which is another factor favoring the overcoming of the kinetic barrier and therefore may enhance deposition of gypsum from such mixtures over the end members (Fig. 6A). Reznik et al., 2009a show a similar trend for the Ω and PPt calculations for mixtures between Dead Sea brine and seawater (which relative to Ein Qedem is less saline and more SO_4^{2-} -rich). Their calculation indicates that Dead Sea-seawater mixtures maximal Ω and PPt values are attained at seawater fractions of ~10% and 30%, respectively. Similar trends are observed in our calculations, i.e., in both cases, the Ω maximum is in mixtures with a lower fraction of Ein Qedem brine than the PPt peak (Fig. 6A upper two rows and right most two columns).

The role of temperature changes is also considered (see Fig. 6D, E). The temperature of Ein Qedem has remained constant at 45° C since first measured, and there is no reason to assume that it has changed much in the past. In contrast, the temperature of the Dead Sea's end member was taken to be in the range of 20° C -45° C (the latter extending the Dead Sea's epilimnion's summer temperature to

Fig. 6. Simulated mixing of Ein Qedem (EQ) with Dead Sea (DS) brines showing various parameters versus the weight fraction of EQ in the mixture (f_{EO}). The notations used in the figure are: Ω - degree of saturation with respect to gypsum; PPt - gypsum precipitation potential in mol·kg H_2O^{-1} , and $\delta^{34}S$ - sulfur isotopic composition. (A) Four scenarios for DS composition with different SO_4^{2-} concentration were simulated (left to right columns): (1) DS composition in 1960 (Neev and Emery, 1967), (2) DS composition in 2008 (Reznik et al., 2009b), (3) DS composition in 2008 with SO_4^{2-} mass equivalent to that in 1960 (i.e., assuming no gypsum precipitated since 1960, and SO_4^{2-} concentration increased in proportion to the decrease in volume due to excess evaporation); and (4) same as scenario #3 but with just half of the SO₄² increase. Four different SO₄² concentration scenarios of EQ brine were considered (the four line colors): (1) EQ brine as measured in the springs system over the past four decades (Weber et al., 2018, Table 1) (red lines); (2) same as #1 but with addition of SO₄²⁻ equivalent to its H_2S concentration (blue lines); (3) same as #1 but with SO_4^{2-} concentration at saturation with respect to gypsum (green lines); and (4) same as #1 but with SO_4^{2-} concentration that will lead it to Ω =1.2 (supersaturation, similar to that of DS in 1960, yellow lines). The gray area indicates the range of $\delta^{34}S_{SO_4}$ values measured on the gypsum samples (Table 2). (B) Ω for three mixing scenarios: (1) DS composition in 2008 (Reznik et al., 2009b) and EQ brine as measured in the springs system over the past four decades (Weber et al., 2018) (dashed lines); (2) mixture of the DS composition in 2008 and the EQ composition in saturation with respect to gypsum (black lines), and (3) mixture of the DS composition in 2008 containing the SO_4^{2-} mass of 1960 and the EQ composition in saturation with respect to gypsum (dotted lines). (C) The same as B but for PPt; (D) The effect of temperature on Ω for scenario DS #4 and EQ #1. (E) The effect of temperature on PPt for scenarios DS #4 and EQ #1. The different lines in D and E represent the different temperatures.

◂

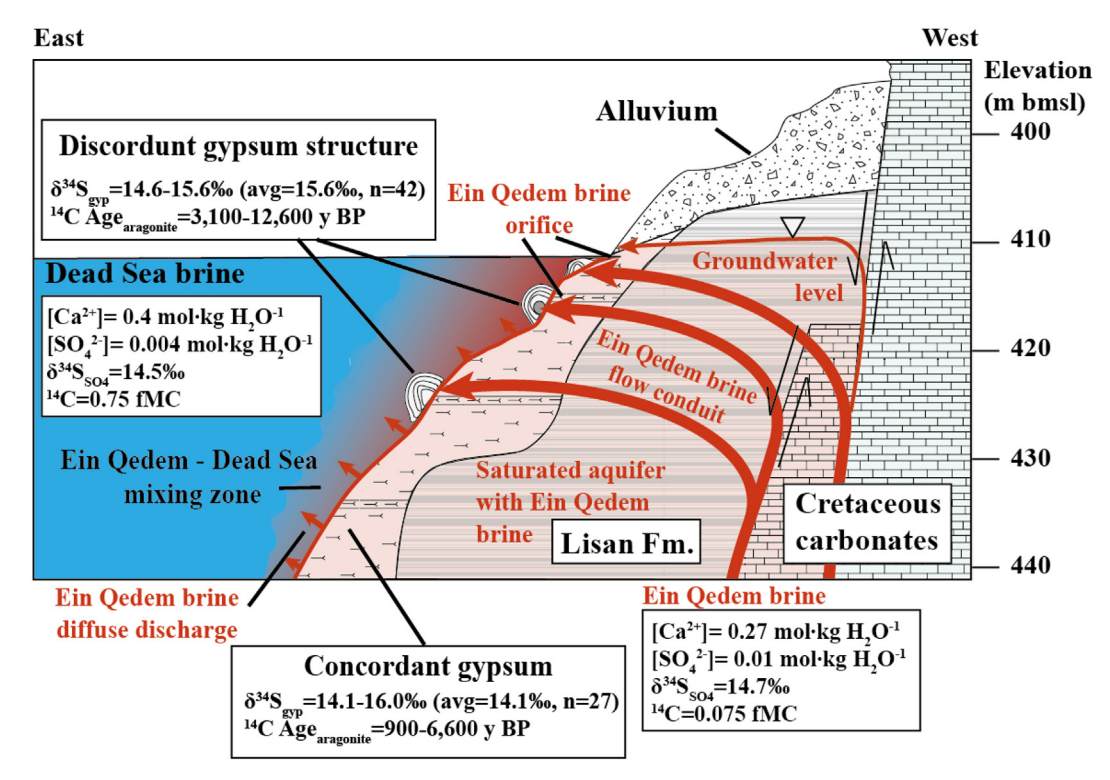


Fig. 7. Schematic west (right) - east (left) cross-section through Cape Qedem during the gypsum deposition periods (modified from Weber et al., 2021). From west to east: Carbonate rocks of the Judea Group, major fault lines of the Dead Sea escarpment west of the Dead Sea, the last Glacial sediments of the Lisan Fm., the unconformity between Lisan Fm. and the overlaying gypsum-rich layers of Cape Qedem, the discordant concentric gypsum mounds that formed around the orifices of the saline springs that discharge the Ein Qedem brine at the Dead Sea margins. The brine (thick solid red lines) rises from a depth of \sim 1 km along the fault plain, filling the coastal aquifer (pink area) and the mixing of its diffused flow with Dead Sea brine, deposited the stratigraphic gypsum at the shoreline and just below forming the distinct "gypsum delta" called Cape Qedem. The Ein Qedem geochemical data provided in the plate, are the values estimated for the time of the gypsum precipitation during the Holocene and are not the present brine values. The ¹⁴C aragonite ages of the gypsum units are the apparent ages (t_{app} , see Fig. 4 and Section 5.1).

account for extreme conditions). At lower temperatures in the Dead Sea, the Ω and PPt slightly rise, but overall, the trend remains quite similar, and the temperature does not significantly impact the conditions for gypsum precipitation.

Mixing the 1960 Dead Sea, as a representative of the Holocene lake during high stands with lower salinity and higher SO_4^{2-} concentrations, with the SO_4^{2-} enriched Ein Qedem brine generally does not support gypsum precipitation from the mixtures during high levels (Fig. 6A, left column). The only exception is in the case of supersaturated Ein Qedem, which exhibits a moderate preference for gypsum precipitation in mixtures relative to the Dead Sea itself (right column in Fig. 6A). This finding is consistent with the observations that during higher lake stands little gypsum deposited along the Dead Sea shores, if at all (Weber et al., 2021).

5.2.5. $\delta^{34}S_{SO_4}$ in the brine and role of BSR in the saline springs' chemistry

The radiocarbon content in the aragonite material within the gypsum structures (Fig. 4) indicates that the solution that precipitated the gypsum-discordant structures comprised up to 30% of Ein Qedem type brine to the solu-

tion precipitating the sedimentary gypsum discordant structures. This evidence is corroborated by the thermodynamic simulations (Fig. 6), showing that the Ω and the PPt values are higher in mixtures containing 10–30% Ein Qedem brine (f_{EQ} of 0.1–0.3). This evaluation is corroborated by the $\delta^{34}S_{SO_4}$ of the gypsum (Fig. 3 and bottom row in Fig. 6A). The $\delta^{34}S_{SO_4}$ average value of the Ein Qedem brine is 24.5%, based on 15 water samples from springs, underwater springs, and a well that were measured as part of this study (Table 1). The $\delta^{34}S_{SO_4}$ of the Ein Qedem brine prior to the BSR was back calculated by the Rayleigh distillation equation:

$$\delta^{34}S_{SO_4} = \delta^{34}S_{SO_4i} + 1000(\alpha - 1)lnf \tag{4}$$

Where $\delta^{34}S_{SO_4i}$ is the $\delta^{34}S_{SO_4}$ of the initial solution, α is the BSR fractionation factor, and f is the fraction of the remaining SO_4^{2-} in solution. For our calculation $\delta^{34}S_{SO_4}$ is the current Ein Qedem value of 24.5%, $\alpha=0.96$ (based on $\Delta=(\delta^{34}S_{SO_4}-\delta^{34}S_{H_2S})$) in the Ca-chloride brines around the Dead Sea (Gavrieli et al., 2001), and f is the ratio between the current SO_4^{2-} concentration in Ein Qedem brine and the initial Ein Qedem sulfate that contains also the additional SO_4^{2-} ($f=\frac{SO_4^{2-}}{SO_4^{2-}+additionalSO_4^{2-}}$) as represented

by the 4 scenarios at the top of Section 5.2.3. Scenario #2 is adding the current sulfide (assuming that it stems from SO_4^{2-} BSR reduction) to the current SO_4^{2-} , in this case: $f = \frac{SO_4^{2-}}{SO_4^{2-} + H_2S}$. For this scenario $\delta^{34}S_{SO_4i}$ of the Ein Qedem brine must have been lower, suggesting that the $\delta^{34}S_{SO_4}$ of the springs was closer to that of the Dead Sea, and that the $\delta^{34}S_{SO_4}$ in the mixtures were closer to those of the gypsum samples ((lower row of Fig. 6A and Fig. 7). The $\delta^{34}S_{SO_4i}$ of Ein Qedem brine in the four scenarios is depicted in Fig. 6A (lower row) at EQ fraction = 1.

The calculated isotopic compositions in the various theoretical mixtures were compared to the isotopic composition obtained from the analyzed gypsum samples (gray shade in in the lower row of Fig. 6A). It can be seen that the gypsum values (14.1–16.9‰) overlap the areas with less than $\sim 30\%$ of Ein Qedem brine in the mixture considering conservative cases in terms of SO₄²⁻ addition to the Ein Qedem brine (Fig. 6A, B, C). In the other cases of higher SO₄²⁻ concentration in Ein Qedem brine (saturation and supersaturation, yellow and green lines, same isotopic composition in Fig. 6A), the calculated $\delta^{34}S_{SO_4}$ are too low to explain the formation of the higher gypsum $\delta^{34}S_{SO_4}$ values. Yet, considering the effect of mass-dependent isotopic fractionation during gypsum precipitation from the brine should bring the gray area to lower values (Fig. 6A bottom) line). The main implication of this analysis is that the chemistry of the Ein Qedem brine could have been modified over time in the subsurface. The brine lost its SO_4^{2-} to BSR until it reached a stage when gypsum could no longer precipitate from the mixtures and gypsum deposition at the vicinity of the springs ceased.

Our explanation for the sulfur and oxygen isotopic compositions and the thermodynamic and kinetic conditions for gypsum precipitation in mixtures of the Dead Sea and Ein Qedem brines requires higher SO_4^{2-} in the saline groundwater, which most likely had experienced earlier active BSR. The presence of sulfide, ammonia and the enrichment in sulfur isotopic composition indicates that BSR is an essential pathway in the evolution of Ein Oedem brine. Previous studies showed that BSR also occurs in shallow and more saline groundwater in the regional aquifer adjacent to the Dead Sea (Gavrieli et al., 2001; Avrahamov et al., 2014). Avrahamov et al., (2014) suggested that the two major factors controlling the reducing conditions in the Dead Sea area are salinity and methane availability. Gavrieli et al., (2001) proposed that the source of reactive organic matter to the deep Ca-chloride brines in the deep Dead Sea Rift is the Upper Cretaceous bituminous rocks, but also oils and asphalts that occur in the Dead Sea area might be involved in the process. In the latter cases, the BSR may had a lower oxidation rate than methane oxidation (Avrahamov et al., 2014).

5.3. Hydrological insights on the brine flow in the Dead Sea coastal aquifer

The models that simulated gypsum precipitation on the Dead Sea margins as depicted in Fig. 7 (e.g., Section 5.2.4) show that SO_4^{2-} concentration in the Ein Qedem brine (and

in the Dead Sea) during the late Holocene was higher than at present. The isotopic compositions of the brines and the gypsum suggest that BSR was responsible for the SO₄²decrease in the groundwater. Probably, the groundwater sulfate concentration at depth decreased steadily, as time passed, while sulfide concentration rose (though some may have precipitated as sulfide minerals in the subsurface). At some point during the past few hundred years, the sulfate concentration in the springs reached a low threshold, at which gypsum precipitation in the Ein Oedem-Dead Sea mixing zone was no longer enabled. If the source of organic matter for BSR is deep, from fossil organic matter in the Cretaceous organic-rich carbonates (the 'bituminous rocks' or 'oil shales', Gavrieli et al., 2001), it would imply that the Qedem-type brine reservoir came from (or passed through) the same deep source.

An alternative explanation for the decrease in the sulfate of the Ein Qedem brine may be that the subsurface brine, which mixed with the Dead Sea during the Holocene came from a rather shallow depth, above the subsurface BSR zone, but had a different composition than the modern Ein Qedem brine. This scenario implies that the brine that is first to recharge the aquifer (the epilimnion of the last glacial Lake Lisan, Weber et al., 2018) will be the last to discharge out of the aquifer (at present), according to the "last-in, first-out" principle. Following this principle, it is possible that the "younger" (last-in) brine was derived from a shallower sector in the aquifer during the Holocene period, and since had been completely exhausted (first-out). Accordingly, the modern Ein Qedem brine, which penetrated the aguifer during the last glacial (first-in) is ascending from a deeper source where substantial BSR occurred (last-out).

The Ein Qedem brine, the gypsum structures, and the aragonite crusts represent stages in the cycling and evolution of the Ca-chloride brine at the Dead Sea lakes and the adjacent regional aquifers. The regional hydrology controls this evolution that in turn reflects the global climate engines. The relation between the activity of the springs that contribute the brines, and of freshwater springs is a key factor in the Dead Sea system. Both types of springs are currently active in the Ein Gedi and Einot Samar areas (Fig. 1A). Thick crusts of aragonite (not of the sort of the authigenic aragonite within the layers of the gypsum mounds) are ubiquitous along the Dead Sea shores and in the vicinity of freshwater springs discharge. The aragonite crusts deposition follows the deposition of the gypsum structures and marks the resumption of the activity of the freshwater springs. A well-documented example is the appearance of gypsum and aragonite crusts at the late Bronze-Iron Age transition at ~ 3200 yr BP (Kagan et al., 2015). Hence, it is possible that local mixing with freshwater in the shallow aguifer as the Ein Qedem type brine ascended from depth during wetter periods and elevated lake levels diluted the brine and lowered the sulfate concentration and consequently the potential of gypsum precipitation.

The enhanced activity of the saline and freshwater springs at the western margins of the Dead Sea and deposition of aragonite and gypsum reflect hydro-climate conditions in the south Levant region and the Dead Sea watershed. These conditions were impacted by the termination of the African Humid Period. During the late Holocene and resumption of the Mediterranean (cyclonic) rain systems, the drying of the Sahara was reflected in enhanced winter rains and mobilize desert dust towards the East Mediterranean - Levant (Palchan et al., 2018a, b). During the relatively high stand periods of the Holocene, freshwater loaded with bicarbonate and sulfate could replenish the lake with these ions. The high stand periods were characterized by the development of epilimnion as has been suggested for the past few hundred years (Stiller and Chung, 1984). During the low stand periods of the Holocene Dead Sea, the sulfate (that was replenished during the high stands) became more concentrated, as seen by gypsum precipitation in the simulated mixing scenarios depicted in the two right columns of Fig. 6A. It is very likely that the abrupt regional aridity and the drops in lake levels (Weber et al., 2021), triggered the resumption (or enhancement) of the activity of the Ein Qedem type saline springs. In summary, our simulations (Fig. 6A, B, C) show that such events of SO₄²⁻ increase in the Dead Sea (and Ein Qedem), along with enhanced activity of the saline springs, have led (upon mixing of these brines) to the formation of the gypsum structures by the outsalting process.

5.4. Gypsum deposition at the Dead Sea shores – The outsalting process

Gypsum occasionally precipitated from the Ca-chloride brine filling the Dead Sea Basin's hypersaline lakes since the ingression of the Sedom lagoon in the late Miocene. This long-term process would have led to a significant depletion of the Dead Sea brine with respect to SO_4^{2-} . However, the brine has maintained supersaturation with respect to gypsum over long periods (Torfstein et al., 2008; Reznik et al., 2009b; Levy et al., 2019). Consequently, any addition of SO₄² that reaches the lake could potentially cause gypsum precipitation. The primary sources of SO_4^{2-} to the lake since its disconnection from the open sea (the Sedom lagoon) at ~3 Ma (Torfstein et al., 2009) are surface freshwater input from the lake's watershed (e.g., Jordan river, winter floods, Stein et al., 1997; Torfstein et al., 2005; Torfstein et al., 2008), recycling of SO₄²⁻ inside the basin (dissolution of older gypsum and anhydrite, Levy et al., 2019) and saline springs.

In the sections above, we described the appearance of marginal gypsum structures, which were formed during the late Holocene (mainly past \sim 4000 y) in the vicinity of the saline springs. We suggest that the addition of SO_4^{2-} in the outlet of these springs causes immediate gypsum precipitation due to mixing of Ein Qedem and Dead Sea brine a process termed *outsalting*. This process also involves deposition of aragonite due to addition of bicarbonate ions (see Fig. 4B for estimates of f_{EQ} based on ^{14}C dating). The outsalting process creates conditions that favor gypsum nucleation by overcoming the kinetic barriers that exist in the Dead Sea brine itself. Despite the supersaturation of the Dead Sea with respect to gypsum, it lacks sufficient sur-

face area because of its slow nucleation process. Therefore, once gypsum surface area became available, the Dead Sea can continue to precipitate gypsum locally even without a supply of sulfate or dilution by the springs, thereby significantly increasing the formation and expansion of the gypsum structures to form "gypsum deltas" (Figs. 8A, B, a term coined by Weber et al., 2021), as long as the lake remains supersaturated with respect to gypsum. In this model, we suggest two different settings for gypsum formation by lake-groundwater mixing, which occurred at the same location (Fig. 7): (1) The discordant gypsum structures, which were formed at the brine orifices area at the exit point of the preferred groundwater flow path; and (2) The stratigraphic "gypsum capes" were formed in areas of significant diffused submarine groundwater discharge (the "gypsum deltas").

In this paper we showed that an evaporite mineral, such as gypsum, can precipitate in a natural environment on rather large scale, by the outsalting mechanism; and not according to the common scenario for the formation of evaporites deposits, by reaching saturation/supersaturation in a solution which undergoes an evaporative concentration of ions. In the following section we provide literature evidence from different geological/hydrological settings for outsalting of gypsum and halite.

5.5. Other natural geological/hydrological settings of outsalting

Conditions for outsalting of other evaporitic minerals are ideal in the Dead Sea, which maintains saturation with respect to halite (Gavrieli et al., 1989; Gavrieli, 1997; Sirota et al., 2016) and supersaturation with respect to gypsum (Katz et al., 1981; Reznik et al., 2009b; Reiss et al., 2021) and receives similarly saturated to supersaturated brines with slightly different Ca-chloride compositions. The most extreme case of such outsalting is the currently forming halite salt delta, which rapidly develops in the southern shores of the Dead Sea at the mouth of the Arava River and is the only chemically known salt delta in the world (Beyth et al., 1997; Fig. 8). Here, Na-depleted halitesaturated end-brines from the evaporation ponds of the potash industries, flow back to the Dead Sea through the Arava River and mix with the Dead Sea brine. The mixing of these two brines results in halite-supersaturated mixtures and precipitation of massive volumes of halite. Gavrieli (1997) estimated that about 10 million tons of halite precipitate annually by this outsalting process annually, resulting in the rapid propagation of the salt delta northward into the lake (Fig. 8C, D). This anthropogenic outsalting process is being formed by mixing of Dead Sea brine with surface flow of end-brine. The natural outsalting of gypsum, which formed the prominent gypsum deltas (Fig. 8A, B) was a result of mixing of the Dead Sea brine with diffused discharge of Ein Qedem type groundwater during the late Holocene (Fig. 7 and Fig. 8A, B). The discordant gypsum bodies (Fig. 4B) were deposited around the springs' discharge orifices (Fig. 7). This mechanism agrees well with the fact that the Ein Qedem brines are hydrothermal, ascending from depth and discharge close to the Dead

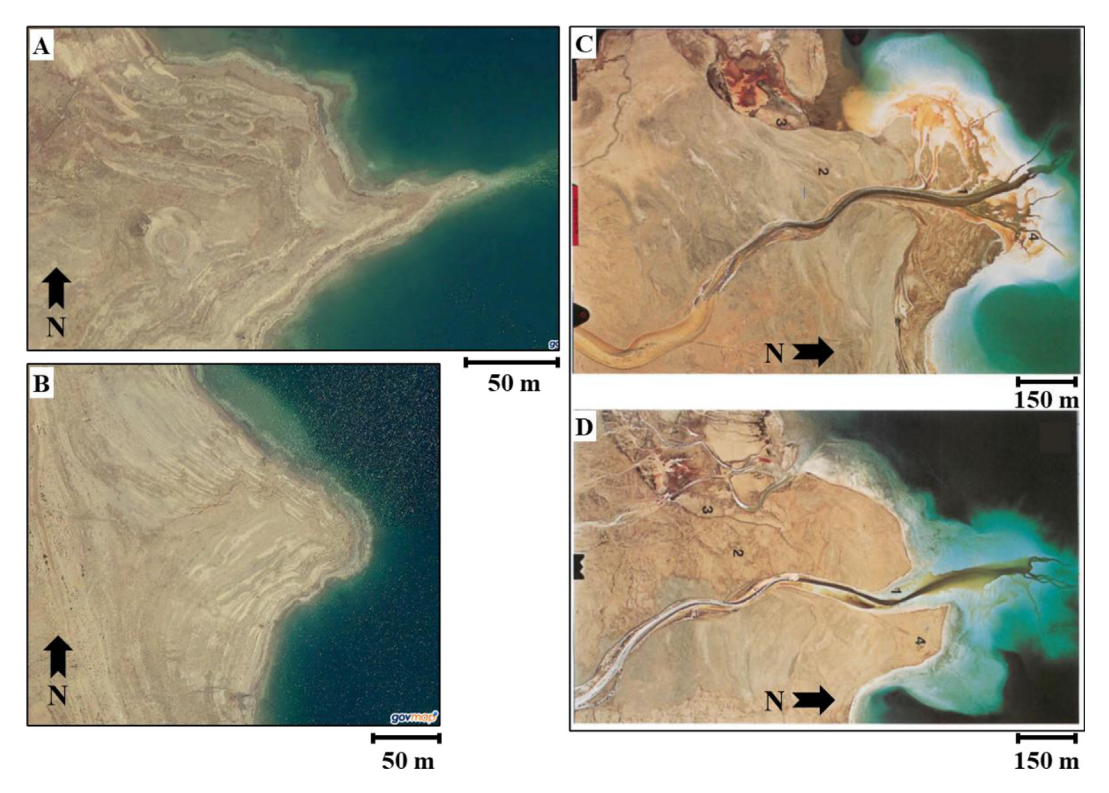


Fig. 8. Aerial photographs of the "deltas" features: (A) and (B) the "gypsum deltas" from Tmarim and Qedem shores, respectively (from govmap, Survey of Israel, 2019); (C) and (D) the "Salt (halite) delta" of Nahal HaArava (the photos were taken in 1989 and 1991, respectively, from Beyth et al., 1997) (locations map in Fig. 1).

Sea shores, often at shallow depths close to lake's level. These characteristics of the outsalting process were used by us to reconstruct the saline springs activity and lake level fluctuations during the Holocene (Weber et al., 2021).

Mixing of two solutions from different sources, which enhance gypsum supersaturation and precipitation, has been proposed as a gypsum formation mechanism in other natural environments worldwide. For example, in the Naica Mine, Mexico, the location of world's largest (several meter long) gypsum crystals were precipitated by mixing of shallow saline waters of evaporative origin, with the regional deep phreatic fluids (Garofalo et al., 2010). Another case is related to the gypsum formation in El Orón-Arco Cave, SE Spain. It has been suggested that gypsum precipitation there involved mixing of seawater and meteoric water seepages to the cave. This mechanism involved oxidation of ³⁴S-depleted sulfide to sulfate in deeper strata, mobilizing this solution to the cave level and precipitating gypsum by mixing with marine water (Gázquez et al., 2019). Gypsum precipitation by outsalting was also reported in coastal aquifer that was affected by seawater intrusion that induced mixing of seawater with freshwater (Gomis-Yagües et al., 2000). In that case a depletion in SO_4^{2-} as compared to a conservative mixing of freshwater and seawater was attributed to gypsum precipitation, which fits our definition of

Finally, we think the mechanism that is suggested in our study may have potential implications for the formation of the thick sequences of gypsum that were deposited in the marginal basins of the Mediterranean during the Messinian Salinity Crisis (MSC, ~5.9–5.6 Ma). The MSC was characterized by a significant retreat of the Mediterranean Sea that was accompanied by deposition of thick evaporitic sequences of halite and gypsum (e.g., Hsü et al., 1973; Ryan, 1973; Roveri et al., 2014a; Meilijson et al., 2018). ⁸⁷Sr/⁸⁶Sr isotope ratios of gypsum from several marginal basins of the Mediterranean are lower than those of contemporaneous open marine environments (e.g., Roveri et al., 2014b; Schildgen et al., 2014; Evans et al., 2015). This change could reflect input of "continental waters", yet the areas circumscribing the Mediterranean were under arid climate conditions during the MSC period (e.g., Rozenbaum et al., 2021). An alternative possibility to explain the precipitation of gypsum with lower than contemporaneous open seawater 87Sr/86Sr ratios, is that evaporated Mediterranean seawater (in marginal basins) mixed with gypsum-saturated saline waters from "continental lagoons" with low 87Sr/86Sr ratios (e.g., Stein et al., 2000). Mixing of these saline waters with contemporaneous Mediterranean evaporated seawater could have triggered the gypsum deposition in the marginal basins by outsalting.

6. SUMMARY AND CONCLUSIONS

The rapid retreat of the Dead Sea during the past decades, led to the exposure of the sedimentary sequences of the Ze'elim Formation that were deposited in the lake during the Holocene. This paper focuses on the mechanism of

deposition of the unique sequences of gypsum that comprise the Ze'elim Formation at the Qedem shore, the western side of the Dead Sea, where the Ein Qedem hot saline springs are discharging an ancient (last glacial) Ca-chloride brine to the Dead Sea.

The sedimentary section at the Qedem shore exposes abundant massive gypsum units with layers containing large bladed gypsum crystals as well as sequences of couplets or triplets of silty detritus, aragonite and gypsum laminae that characterized the typical lacustrine sedimentary facies of the Holocene Dead Sea. The thick gypsum units were deposited in a stratigraphic order on an erosional unconformity that cut through the last glacial Lisan Formation. Gypsum also appears in places as thick crusts, which cover discordantly the stratigraphic units of the last glacial Lisan Formation and the early to mid-Holocene Ze'elim Formation. The thick gypsum units and discordant gypsum crusts form a prominent topographic feature, a gypsum delta, termed "the Cape Qedem". In addition, the Qedem shore is pitted with isolated unique gypsum structures ("mounds") that contain some authigenic aragonite. Similar structures are ubiquitous along the western shores of the Dead Sea from Ein Gedi to Einot Zugim.

The outcrops of "Cape Qedem" and the isolated gypsum mounds were dated by radiocarbon using short lived terrestrial organic debris. $\delta^{18}O$ and $\delta^{34}S$ of the gypsum sulfate and the radiocarbon contents in the authigenic aragonite were measured and used to constrain the conditions of gypsum formation.

The main observations and conclusions of the study are:

- 1. The $\delta^{34}S_{gyp}$ and $\delta^{18}O_{gyp}$ isotopic composition of gypsum samples from the "Cape Qedem" and from the isolated gypsum structures from various locations along the Dead Sea western shores show a rather narrow range of values ($\delta^{34}S_{gyp}$: 14.1–16.9%; $\delta^{18}O_{gyp}$: 14.4–16.5%).
- 2. Based on ¹⁴C dating of organic debris within the gypsum structures, their deposition occurred during the past 4,000 years. However, old radiocarbon ages of authigenic aragonite within the gypsum structures indicate contribution of bicarbonate ions by Ein Qedem-type brine that represents the last glacial Lake Lisan. Along with the bicarbonate ions the Ein Qedem type brines also provided sulfate to the lake leading to the formation of the gypsum structures.
- 3. The enhanced activity of the saline springs and mixing of the springs and lake brines during periods of arid conditions and lower lake levels led to the formation of the prominent gypsum deltas and gypsum structures by a process termed "gypsum outsalting".
- 4. Thermodynamic calculations show that under more limited BSR activity in the Ein Qedem brine and with the addition of SO₄²⁻ to mixtures of the Dead Sea and Ein Qedem brines, gypsum precipitation is enabled by mixing of the two brines. Similar process of "halite outsalting" and "salt delta" formation occurs currently at modern Dead Sea where the end-brine that flows on the surface from the industrial evaporation ponds back to the lake mixes with the Dead Sea brine.

- 5. The hydroclimate conditions in the watershed of the Dead Sea (that reflect the conditions in the East Mediterranean-south Levant region) were overall arid during the Holocene, with lake levels lying below ~400 m bmsl. The Holocene aridity was interrupted by wetter intervals at the late Bronze Age, the Roman-Byzantine period, and during the past ~300 years. Then, regional runoff provided bicarbonate and sulfate to the lake allowing the formation of primary aragonite and gypsum.
- 6. Outsalting process of salts could occur in other saline and hypersaline water-bodies, where brines of various salinities mix, e.g., in the Mediterranean Sea during the time of Messinian Salinity Crisis. An assessment of this suggestion is beyond the scope of this study and requires further research.

Declaration of Competing Interest

The authors declare that they have no known competing financial interests or personal relationships that could have appeared to influence the work reported in this paper.

ACKNOWLEDGMENTS

We thank the staff of the National Ocean Sciences Accelerator Mass Spectrometry (NOSAMS) facility, Woods Hole Oceanographic Institution (WHOI), Woods Hole, MA, for providing the first author (NW) working space, helping her in the submission of a successful travel grant and the analytical process. We thank Navot Morag from the Geological Survey of Israel for helping with the quantitative XRD analyses. We thank the Godwin Laboratory for Paleoclimate Research for analysis of the sulfur and oxygen isotopic composition of gypsum, which was funded through NERC grant NE/S001344/1 to A. V. T. We thank the BSF Rahamimoff Travel Grant for Young Scientists, which funded the travel expenses of NW to NOSAMS. The study was supported by the PALEX project "Paleohydrology and Extreme Floods from the Dead Sea ICDP Core", funded by the DFG, Germany (Grant No. BR2208/13-1/-2 to BL and MS) Grants from ISF Center of Excellence (up to end of 2019) and ISF 695/19 (from the end of 2019) to BL and by funds of the Israeli Government under GSI Dead Sea project #40573. Finally, we thank the associate editor and the referees for their comprehensive work that substantially improved the manuscript.

APPENDIX A. DEAD SEA – EIN QEDEM MIXING MODELS

The 14 C content (fMC) of aragonite in a gypsum sample at the time of its precipitation (t_0) is a mixture of two end components - the Dead Sea and Ein Qedem brines:

$$^{14}C_{aragonite,t_0} = ^{14}C_{EQ} \cdot DIC_{EQ} \cdot f_{EQ} + ^{14}C_{DS} \cdot DIC_{DS} \cdot (1 - f_{EQ})$$

$$(A.1)$$

Where 14 C, DIC and f_{EQ} are the radiocarbon content, the dissolve inorganic carbon concentration in the end member brine and the fraction of Ein Qedem brine in the mixture, where the subscripts EQ and DS denote Ein Qedem and the Dead Sea, respectively.

The 14 C content of the authigenic aragonite today (14 C_{aragonite,t}, the 14 C at time t) is measured (where \underline{t} is the time elapsed since the precipitation of the aragonite). In order to evaluate the aragonite 14 C content during its precipitation (at t_0), it is calculated backward from the decay equation of radiocarbon as follows:

$$^{14}C_{aragonite,t_0} = e^{\lambda \cdot t_{real}} \cdot ^{14}C_{aragonite,t} \tag{A.2}$$

Where λ is the Libby decay constant of ¹⁴C (1/8033 yr⁻¹, Stuiver and Polach, 1977) and t_{real} is the "real" ¹⁴C age as measured on the organic debris from the same horizon as the aragonite. In cases that organic debris were not found t_{real} was taken to be 700 yr BP and 2900 yr BP (end of Section 5.1). The estimated ¹⁴C_{aragonite,to} is used to calculate the fraction of Ein Qedem in the sample (f_{EQ}) by substituting Eq. (A.2) into Eq. (A.1) as follows:

$$f_{EQ} = \frac{^{14}C_{DS} \cdot DIC_{DS} - e^{\lambda \cdot t_{real}} \ 14C_{aragonite,t}}{^{14}C_{DS} \cdot DIC_{DS} - ^{14}C_{EQ} \cdot DIC_{EQ}} \tag{A.3} \label{eq:equation:equat$$

2. For the thermodynamic and kinetic model of gypsum precipitation from the Dead Sea–Ein Qedem mixtures (Fig. 6), the major ions composition in the mixture was calculated separately for each ion for any $f_{\rm EQ}$ between 0 to 1 by a simple mixing equation:

$$\mathbf{x}_{i,\text{mix}} = \mathbf{f}_{EO} \cdot \mathbf{x}_{i,EO} + (1 - \mathbf{f}_{EO}) \cdot \mathbf{x}_{i,DS} \tag{A.4}$$

Where x_i denotes each of the major ions in Table 1 for the Ein Qedem and the Dead Sea composition. All relevant thermodynamic parameters (e.g., Ω , PPt) were calculated for every mixture by the PHREEQC code. The $\delta^{34}S_{SO4}$ of the mixtures was calculated by Eq. (A.4).

APPENDIX B. SUPPLEMENTARY DATA

Supplementary data to this article can be found online at https://doi.org/10.1016/j.gca.2021.10.002.

REFERENCES

- Avrahamov N., Antler G., Yechieli Y., Gavrieli I., Joye S. B., Saxton M., Turchyn A. v. and Sivan O. (2014) Anaerobic oxidation of methane by sulfate in hypersaline groundwater of the Dead Sea aquifer. *Geobiology* 12(6), 511-528.
- Babel M. (2007) Depositional environments of a salina-type evaporite basin recorded in the Badenian gypsum facies in the northern Carpathian Foredeep. Geol. Soc. Spec. Pub. 285, 107– 142.
- Belmaker R., Lazar B., Stein M., Taha N. and Bookman R. (2019) Constraints on aragonite precipitation in the Dead Sea from geochemical measurements of flood plumes. *Quat. Sci. Rev.* 221 105876.
- Belmaker R., Stein M., Yechieli Y. and Lazar B. (2007) Controls on the radiocarbon reservoir ages in the modern Dead Sea drainage system and in the Last Glacial Lake Lisan. *Radiocar*bon 49, 969–982.
- Beyth M., Katz O. and Gavrieli I. (1997) Progradation and retrogradation of the Salt Delta in the southern Dead Sea, 1985–1992. Israel J. Earth Sci. 46, 95–106.
- Bookman R., Enzel Y., Agnon A. and Stein M. (2004) Late Holocene lake levels of the dead sea. *Bull. Geolog. Soc. Am.* 116, 555–571.

- Bookman R., Lazar B., Stein M. and Burr G. S. (2007) Radiocarbon dating of primary aragonite by sequential extraction of CO₂. *Holocene* 17, 131–137.
- van Driessche A. E. S., Canals A., Ossorio M., Reyes R. C. and García-Ruiz J. M. (2016) Unraveling the sulfate sources of (giant) gypsum crystals using gypsum isotope fractionation factors. *J. Geol.* **124**, 235–245.
- Evans N. P., Turchyn A. v., Gázquez F., Bontognali T. R. R., Chapman H. J. and Hodell D. A. (2015) Coupled measurements of δ18O and δD of hydration water and salinity of fluid inclusions in gypsum from the Messinian Yesares Member, Sorbas Basin (SE Spain). *Earth and Planetary Science Letters* **430**, 499–510.
- Garofalo P. S., Fricker M. B., Günther D., Forti P., Mercuri A. M., Loreti M. and Capaccioni B. (2010) Climatic control on the growth of gigantic gypsum crystals within hypogenic caves (Naica mine, Mexico)? Earth Planet. Sci. Lett. 289, 560–569.
- Gavrieli I. (1997). Halite deposition in the Dead Sea: 1960-1993. In: The Dead Sea - The Lake and Its setting (eds. Ben-Avraham Z. and Ginzburg A. Niemi T.M.). Oxford University Press, 161-170.
- Gavrieli I., Starinsky A. and Bein A. (1989) The solubility of halite as a function of temperature in the highly saline Dead Sea brine system. *Limnol. Oceanogr.* 34(7), 1224–1234.
- Gavrieli I. and Stein M. (2006) On the origin and fate of the brines in the Dead Sea basin. *Geolog. Soc. Am.* **2401**, 1–22.
- Gavrieli I., Yechieli Y., Halicz L., Spiro B., Bein A. and Efron D. (2001) The sulfur system in anoxic subsurface brines and its implication in brine evolutionary pathways: the Ca-chloride brines in the Dead Sea area. Earth Planet. Sci. Lett. 186, 199– 213
- Gázquez F., Calaforra J. M., Evans N. P., Turchyn A. v., Rull F., Medina J., Ros A., Llamusí J. L., Sánchez J. and Hodell D. A. (2019) Physical weathering of carbonate host-rock by precipitation of soluble salts in caves: A case study in El Orón-Arco Cave (Region of Murcia, SE Spain). Chemical Geology 521, 1–11.
- Golan R., Gavrieli I., Ganor J. and Lazar B. (2016) Controls on the pH of hyper-saline lakes – A lesson from the Dead Sea. *Earth Planet. Sci. Lett.* **434**, 289–297.
- Gomis-Yagües V., Boluda-Botella N. and Ruiz-Beviá F. (2000) Gypsum precipitation/dissolution as an explanation of the decrease of sulphate concentration during seawater intrusion. *J. Hydrol.* 228, 48–55.
- Haliva-Cohen A., Stein M., Goldstein S. L., Sandler A. and Starinsky A. (2012) Sources and transport routes of fine detritus material to the Late Quaternary Dead Sea basin. *Quat. Sci. Rev.* 50, 55–70.
- Hsü K. J., Ryan W. B. F. and Cita M. B. (1973) Late miocene desiccation of the mediterranean. *Nature* **242**, 240–244.
- Kagan E. J., Langgut D., Boaretto E., Neumann F. H. and Stein M. (2015) Dead Sea Levels during the Bronze and Iron Ages. *Radiocarbon* 57, 237–252.
- Katz A. and Starinsky A. (2009) Geochemical history of the Dead Sea. *Aquat. Geochem.* **15**, 159–194.
- Katz A., Starinsky A., Taitel-Goldman N. and Beyth M. (1981) Solubilities of gypsum and halite in the Dead Sea and in its mixtures with seawater. *Limnol. Oceanogr.* 26, 709–716.
- Lerman A. (1967) Model of chemical evolution of a chloride lake— The Dead Sea. *Geochim. Cosmochim. Acta* **31**, 2309–2330.
- Levy E. J., Sivan O., Antler G., Lazar B., Stein M., Yechieli Y. and Gavrieli I. (2019) Mount Sedom salt diapir Source for sulfate replenishment and gypsum supersaturation in the last glacial Dead Sea (Lake Lisan). *Quat. Sci. Rev.* **221** 105871.
- Levy E. J., Yechieli Y., Gavrieli I., Lazar B., Kiro Y., Stein M. and Sivan O. (2018) Salt precipitation and dissolution in the late

- Quaternary Dead Sea: Evidence as deduced from the chemical and δ^{37} Cl composition of pore fluids and halites. *Earth Planet. Sci. Lett.* **487**, 127–137.
- Machlus M., Enzel Y., Goldstein S. L., Marco S. and Stein M. (2000) Reconstructing low levels of Lake Lisan by correlating fan-delta and lacustrine deposits. *Quat. Int.* **73**, 137–144.
- Mazor E. and Mero F. (1969) The origin of the Tiberias-Noit mineral water association in the Tiberias-Dead Sea Rift Valley, Israel. *J. Hydrol.* **7**, 318–333.
- Meilijson A., Steinberg J., Hilgen F., Bialik M., Waldmann N. D. and Makovsky Y. (2018) Deep-basin evidence resolves a 50-year-old debate and demonstrates synchronous onset of messinian evaporite deposition in a non-desiccated mediterranean. *Geology* 46, 243–246.
- Migowski C., Stein M., Prasad S., Negendank J. F. W. and Agnon A. (2006) Holocene climate variability and cultural evolution in the Near East from the Dead Sea sedimentary record. *Quat. Res.* **66**, 421–431.
- Müller G. and Gastner M. (1971) The "Karbonat-Bombe", a simple device for the determination of carbonate content in sediment, soils, and other materials, Neues Jahrbuch für Mineralogie Monatshefte, Bremerhaven. *Pangaea* 10, 466–469.
- Neev D. and Emery K. O. (1967) The Dead Sea Depositional processes and environments of evaporites. *Geol. Surv. Isr. Bull.* 41, 1–147.
- Nissenbaum, A., Kaplan, I. R., (1976). Sulfur and carbon isotopic evidence for biogeochemical processes in the Dead Sea ecosytem. In: J.O Nriagu (Ed.), *Environmental Biogeochemistry*, Ann Arbor Science, vol. 1, pp. 309–325.
- Palchan D., Erel Y. and Stein M. (2018a) Geochemical characterization of contemporary fine detritus in the Dead Sea watershed. Chem. Geol. 494, 30–42.
- Palchan D., Stein M., Goldstein S. L., Almogi-Labin A., Tirosh O. and Erel Y. (2018b) Synoptic conditions of fine-particle transport to the last interglacial Red Sea-Dead Sea from Nd-Sr compositions of sediment cores. *Quat. Sci. Rev.* 179, 123–136.
- Parkhurst, D. L. and Appelo, C. A. J. (1999) PHREEQC 2.15 a computer program for speciation, batch-reaction, one-dimentional transport and inverse geochemical calculation. *Water-Resources Investigation Report* 99–4259. U.S. Geological Survey.
- Reiss A. G., Gavrieli I., Rosenberg Y. O., Reznik I. J., Luttge A., Emmanuel S. and Ganor J. (2021) Gypsum precipitation under saline conditions: Thermodynamics, kinetics, morphology, and size distribution. *Minerals* 11, 1–38.
- Reznik I. J., Ganor J., Gal A. and Gavrieli I. (2009a) Gypsum saturation degrees and precipitation potentials from Dead Seaseawater mixtures. *Environ. Chem.* **6**, 416.
- Reznik I. J., Gavrieli I. and Ganor J. (2009b) Kinetics of gypsum nucleation and crystal growth from Dead Sea brine. Geochim. Cosmochim. Acta 73, 6218–6230.
- Roberts M. L., Beaupré S. R. and Burton J. R. (2013) A High-Throughput, Low-Cost Method for Analysis of Carbonate Samples for ¹⁴C. *Radiocarbon* 55, 585–592.
- Roveri M., Flecker R., Krijgsman W., Lofi J., Lugli S., Manzi V., Sierro F. J., Bertini A., Camerlenghi A., de Lange G., Govers R., Hilgen F. J., Hübscher C., Meijer P. T. and Stoica M. (2014a) The messinian salinity crisis: past and future of a great challenge for marine sciences. *Marine Geology* 352, 25–58.
- Roveri M., Lugli S., Manzi V., Gennari R. and Schreiber B. C. (2014b) High-resolution strontium isotope stratigraphy of the Messinian deep Mediterranean basins: Implications for marginal to central basins correlation. *Marine Geology* 349, 113–125.

- Rozenbaum A. G., Sandler A., Stein M. and Zilberman E. (2019) The sedimentary and environmental history of Tortonian-Messinian lakes at the east Mediterranean margins (northern Israel). *Sed. Geol.* **383**, 268–292.
- Rozenbaum A. G., Stein M., Zilberman E., Shaked Gelband D., Starinsky A. and Sandler A. (2021) Sr isotopes in the Tortonian-Messinian Lake Bira and Gesher marshes, Northern Valleys of Israel: Implications for hydroclimate changes in East Mediterranean—Levant margins. *GSA Bulletin*, 1–14.
- Ryan W. B. F. (1973) Geodynamic implications of the Messinian crisis of salinity. In *Messinian Events in the Mediterranean* (ed. C. W. Drooger). North-Holland Publishing Company, Amsterdam, pp. 26–38.
- Schildgen T. F., Cosentino D., Frijia G., Castorina F., Dudas F.
 Ö., Iadanza A., Sampalmieri G., Cipollari P., Caruso A.,
 Bowring S. A. and Strecker M. R. (2014) Sea level and climate forcing of the Sr isotope composition of late Miocene Mediterranean marine. *Journal of African Earth Sciences* 30, 865–886
- Shalev E. and Yechieli Y. (2007) The effect of Dead Sea level fluctuations on the discharge of thermal springs. *Israel J. Earth Sci.* **56**, 19–27.
- Sirota I., Arnon A. and Lensky N. G. (2016) Seasonal variations of halite saturation in the Dead Sea. *Water Resour. Res.* **52**, 7151–7162
- Smoot J. P. and Lowenstein T. K. (1991) Chapter 3 Depositional Environments of Non-Marine Evaporites. *Developments in Sedimentology* 50, 189–347.
- Starinsky A. (1974) Relationship between Ca-Chloride Brines and Sedimentary Rocks in Israel Ph D thesis. Hebrew University of Jerusalem.
- Starinsky A. and Katz A. (2014) *The Story of Saline Water in the Dead Sea Rift The Role of Runoff and Relative Humidity*. Reviews, In Dead Sea Transform Fault System, pp. 317–353.
- Stein M. (2014) The Evolution of Neogene-Quaternary Water-Bodies in the Dead Sea Rift Valley. In Springer, Dordrecht, pp. 279–316.
- Stein M. (2001) The sedimentary and geochemical record of neogene-quaternary water bodies in the Dead Sea basin -Inferences for the regional paleoclimatic history. In. J. Paleolimnol., 271–282.
- Stein M., Agnon A., Katz A. and Starinsky A. (2002) Strontium isotopes in discordant dolomite bodies of the Judea Group, Dead Sea basin. *Israel J. Earth Sci.* **51**, 219–224.
- Stein M., Lazar B. and Goldstein S. L. (2013) Radiocarbon Reservoir Ages as Freshwater-Brine Monitors in Lake Lisan, Dead Sea System. *Radiocarbon* 55, 1050–1057.
- Stein M., Starinsky A., Agnon A., Katz A., Raab M., Spiro B. and Zak I. (2000) The impact of brine-rock interaction during marine evaporite formation on the isotopic Sr record in the oceans: evidence from Mt. Sedom Israel. *Geochimica et Cosmochimica Acta* 64, 2039–2053.
- Stein M., Starinsky A., Katz A., Goldstein S. L., Machlus M. and Schramm A. (1997) Strontium isotopic, chemical, and sedimentological evidence for the evolution of Lake Lisan and the Dead Sea. *Geochim. Cosmochim. Acta* 61, 3975–3992.
- Steinhorn I., Assaf G., Gat J. R., Nishry A., Nissenbaum A., Stiller M., Beyth M., Neev D., Garber R., Friedman G. M. and Weiss W. (1979) The Dead Sea: Deepening of the Mixolimnion Signifies the Overture to Overturn of the Water Column. Science 206, 55–57.
- Stiller M. and Chung Y. C. (1984) Radium in the Dead Sea: A possible tracer for the duration of meromixis 1. *Limnol. Oceanogr.* **29**, 574–586.
- Stuiver M. and Polach H. A. (1977) Discussion Reporting of ¹⁴C Data. *Radiocarbon* **19**, 355–363.

- Talma A. S., Vogel J. C. and Stiller M. (1997) *The radiocarbon content of the Dead Sea*. The lake and its setting, The Dead Sea, pp. 171–183.
- Torfstein A., Gavrieli I., Katz A., Kolodny Y. and Stein M. (2008) Gypsum as a monitor of the paleo-limnological–hydrological conditions in Lake Lisan and the Dead Sea. *Geochim. Cosmochim. Acta* 72, 2491–2509.
- Torfstein A., Gavrieli I. and Stein M. (2005) The sources and evolution of sulfur in the hypersaline Lake Lisan (paleo-Dead Sea). *Earth Planet. Sci. Lett.* **236**, 61–77.
- Torfstein A., Haase-Schramm A., Waldmann N. D., Kolodny Y. and Stein M. (2009) U-series and oxygen isotope chronology of the mid-Pleistocene Lake Amora (Dead Sea basin). *Geochim. Cosmochim. Acta* **73**, 2603–2630.
- Warren J. K. (2016) Evaporites: A geological compendium. Springer.
- Warren J. K. (1982) The hydrological setting, occurrence and significance of gypsum in late Quaternary salt lakes in South Australia. *Sedimentology* **29**, 609–637.

- Weber N., Lazar B., Gavrieli I., Yechieli Y. and Stein M. (2021) Gypsum Deltas at the Holocene Dead Sea Linked to Grand Solar Minima. *Geophys. Res. Lett.* **48**, 1–10.
- Weber N., Lazar B., Stern O., Burr G., Gavrieli I., Roberts M., Kurz M. D., Yechieli Y. and Stein M. (2020) Radiocarbon Reservoir Ages in The Holocene Dead Sea. *Radiocarbon* 62, 1453–1473.
- Weber N., Yechieli Y., Stein M., Yokochi R., Gavrieli I., Zappala J., Mueller P. and Lazar B. (2018) The circulation of the Dead Sea brine in the regional aquifer. *Earth Planet. Sci. Lett.* 493, 242–261.
- Yechieli Y., Magaritz M., Levy Y., Weber U., Kafri U., Woelfli W. and Bonani G. (1993) Late Quaternary Geological History of the Dead Sea Area, Israel. *Quat. Res.* **39**, 59–67.
- Zak I. (1967) The Geology of Mt. Sedom. Ph D thesis. Hebrew University of Jerusalem.

Associate editor: Alexandra V. Turchyn